5-10-1996

Prolonged history of silicic peralkaline volcanism in the eastern Pacific Ocean

Wendy A. Bohrson
University of California - Los Angeles

Mary R. Reid
University of California - Los Angeles

Anita L. Grunder
Oregon State University

Matthew Heizler
University of California - Los Angeles

T. Mark Harrison
University of California - Los Angeles

See next page for additional authors

Recommended Citation
Bohrson W.A., Reid M.R., Grunder A.L., Heizler M.T., Harrison T.M., Lee, J. (1996). Prolonged history of silicic peralkaline volcanism in the eastern Pacific Ocean. *Journal of Geophysical Research - Solid Earth, 101*(B5), 11457-11474. DOI: 10.1029/96JB00329

JOURNAL OF GEOPHYSICAL RESEARCH, VOL. 101, NO. B5, PAGES 11,457–11,474, MAY 10, 1996

Prolonged history of silicic peralkaline volcanism in the eastern Pacific Ocean

Wendy A. Bohrson,[1,2] Mary R. Reid,[1] Anita L. Grunder,[3] Matthew T. Heizler,[1,4] T. Mark Harrison,[1] and Jeffrey Lee[5]

Abstract. Socorro Island, Mexico, is an alkaline and peralkaline volcanic island located in the eastern Pacific Ocean on a mid-ocean ridge spreading center that was abandoned at ~3.5 Ma. Silicic peralkaline rocks comprise up to 80% of the surface of the island, rendering Socorro virtually unique in the Pacific Ocean. Precise, replicate $^{40}Ar/^{39}Ar$ ages of 21 peralkaline trachytes and rhyolites reveal a history of episodic volcanic activity from ~540 to 370 ka that may have culminated with caldera formation; repose periods between these episodes may have had maximum duration of ~30 kyr. After up to 200 kyr of quiescence, $^{40}Ar/^{39}Ar$ ages indicate that postcaldera silicic peralkaline activity commenced by 180 ka, forming the Cerro Evermann Formation. Postcaldera mafic alkaline lavas of the Lomas Coloradas Formation erupted dominantly between 70 and 150 ka based upon relative age relations. The dominant lithology of precaldera and syncaldera silicic peralkaline deposits on Socorro is nonfragmental and nonvesicular and lacks lithic fragments and fiamme; despite this, numerous lines of evidence including welding zonation, presence of a proximal ignimbrite or co-ignimbrite deposit, association with a caldera, and compositional heterogeneity within eruptive units suggest that they are dominantly ash flow tuffs. A change in eruptive style, from predominantly explosive to predominantly effusive, followed caldera formation and suggests that a change in the efficacy of magma degassing may be linked to caldera formation. On the basis of the presence of a caldera, the magma chamber associated with Socorro Island is shallow and probably resides within the upper oceanic crust or the edifice. This together with a prolonged history of silicic magmatism indicates that intrusion of mafic magma maintained thermal viability of the magmatic plumbing system. The minimum calculated growth rate for the entire volcanic edifice ($7x10^{-4}$ km^3/yr) exceeds those of nonhotspot off-axis volcanoes in the Pacific by almost an order of magnitude. Eruption rates for subaerial phases on Socorro may be several orders of magnitude smaller than this growth rate and are comparable to subaerial eruption rates of isolated ocean islands related to mantle plumes.

Introduction

The northern Mathematicians Ridge (inset, Figure 1) marks the location of a mid-ocean ridge spreading center that was abandoned at ~3.5 Ma when activity shifted to the East Pacific Rise [*Mammerickx et al.*, 1988]. At the northern terminus of the ridge, Socorro and three other alkaline volcanic islands (San Benedicto, Clarion, and Roca Partida) comprise the Revillagigedo archipelago; except for Roca Partida, the islands have volumes in the upper 1-2% of Pacific seamounts and islands on Pliocene age oceanic crust [*Batiza*, 1982]. Together with numerous seamounts in the Mathematicians Ridge [*Batiza and Vanko*, 1985], the Revillagigedo archipelago represents postabandonment alkaline magmatism. Volcanic activity in this region has continued to the present as demonstrated by a submarine basalt eruption ~3 km west of Socorro Island in January 1993 [*McClelland et al.*, 1993; *Siebe et al.*, 1995]. Other evidence that the area has been recently active includes eruption of San Benedicto Island in 1952-1953 [*Richards*, 1959], minor eruptive activity on Socorro Island in 1951 [*Crowe and Crowe*, 1955], a ~5 ka radiocarbon age for a lacustrine deposit stratigraphically underlying a basaltic cone on Socorro Island [*Farmer et al.*, 1993], and young ages of submarine volcanic rocks inferred from manganese crust thicknesses (J. Hein, written communication, 1991) and He isotope data [*Graham et al.*, 1988].

Socorro Island is virtually unique in the Pacific Basin, being one of the few volcanic islands dominated by subaerial eruptions of silicic peralkaline composition. In this study, we present detailed mapping, lithofacies, stratigraphic, and $^{40}Ar/^{39}Ar$ chronological data for rocks from the southeastern quadrant of Socorro Island, where precaldera, syncaldera, and postcaldera deposits are relatively well exposed. In addition to establishing an eruptive chronology for the volcanic deposits on the island, these data quantify eruption rates, eruption durations, and magma volumes of an oceanic silicic peralkaline volcano, establish the framework by which to assess temporal changes in eruptive style and eruption rates, and allow general inferences to be made about the magma reservoir. We compare eruption and growth rates of volcanoes with known sources (e.g., off-axis seamounts, volcanoes

[1]Department of Earth and Space Sciences, University of California, Los Angeles.
[2]Now at Department of Geological Sciences, University of California, Santa Barbara.
[3]Department of Geosciences, Oregon State University, Corvallis.
[4]Now at New Mexico Bureau of Mines and Mineral Resources, Socorro.
[5]Geology Department, Central Washington University, Ellensburg.

Paper number 96JB00329.
0148-0227/96/96JB-00329$09.00

related to mantle plumes) to those of Socorro in order to try to constrain the source of alkaline magmatism in this abandoned ridge setting.

Previous Work

The eruptive history of Socorro Island was divided into precaldera and postcaldera stages by *Bryan* [1959, 1966, 1976] (Figure 1). Precaldera stage rocks, exposed dominantly on the eastern side of the island, were characterized as products of effusive eruptions ranging from volumetrically dominant, older alkalic basalt to rare, younger comendite (peralkaline rhyolite). A summit caldera was identified, although syncaldera deposits were not. Postcaldera phase rocks were divided into the Cerro Evermann and Lomas Coloradas Formations on the basis of composition and location (Figure 1). Rocks of the Cerro Evermann Formation, dominantly silicic peralkaline domes and lava flows with minor alkalic basalt flows and cones, are exposed in the caldera as well as on the northern, western, and southern flanks. The Lomas Coloradas Formation comprises dominantly alkaline basalt flows and cones confined to the southeastern quadrant. In addition, several trachyte domes located near the southeastern coast were included in the Lomas Coloradas Formation. *Bryan* [1959] could not decipher relative ages between rocks of the Cerro Evermann and Lomas Coloradas Formations but suggested that eruptions of the two formations may have been contemporaneous.

Field and $^{40}Ar/^{39}Ar$ Methods

Seven weeks during 1990 and 1991 were spent mapping and sampling the southeastern quadrant of Socorro Island (Figures 1 and 2) where great compositional diversity (alkalic basalt to peralkaline rhyolite), the greatest temporal range, and the least vegetation occur. Correlation of postcaldera flows and vents was possible using phenocryst assemblage, flow lithology, and location. Relative stratigraphy for postcaldera deposits was established using relationships observed in stream drainages and at contacts between deposits. The $^{40}Ar/^{39}Ar$ ages confirmed the relative stratigraphic relations of these units observed in the field. In distinct contrast, correlation of precaldera and syncaldera deposits was difficult due to similarities of their lithologic characteristics (e.g., phenocryst assemblage, degree of weathering, and vesicularity). Stratigraphic relations were generally not established in the field because the deposits are lithologically similar and because exposure of an individual deposit was typically discontinuous, probably due to both erosion and its original distribution. For precaldera and syncaldera deposits, $^{40}Ar/^{39}Ar$ ages were used to define the stratigraphy.

Alkali feldspar (K_2O range: 5-6 wt %) separates from 30 whole rock samples were obtained by crushing, magnetic separation, and hand picking to >99% purity. For ash flow tuffs, whole rock feldspar separates were used because fiamme or pumice are largely absent, and in cases where they are present, they are extensively altered. Feldspar separates that had visible alteration were cleaned ultrasonically in ~10% HF for 1-3 min and were rinsed several times in distilled water. The 100 to 150 mg separates were wrapped in aluminum foil, sealed in evacuated pyrex tubes, and irradiated in the University of Michigan Ford reactor (site L67, power level 2 MW) for 3 hours. Because of the large sample size, Fish Canyon Tuff sanidine (27.8 Ma [*Miller et al.*, 1985]) flux monitors were interleaved every 5 mm (n=10) in order to monitor neutron flux gradients. J factors were determined by averaging three analyses, each performed on a single 20-28 mesh crystal; reproducibility was ±0.5% ($1\sigma_{S.D.}$). Measured irradiation parameters for CaF_2 and K_2SO_4 are $(^{36}Ar/^{37}Ar)$ = 0.00029, $(^{39}Ar/^{37}Ar)_{Ca}$ = 0.0007, and $(^{40}Ar/^{39}Ar)_K$ = 0.001±0.015; the $(^{40}Ar/^{39}Ar)_K$ and associated uncertainty reflect shielding of thermal neutrons by (borated) pyrex tubes and the high atmospheric contamination of K_2SO_4. If a $(^{40}Ar/^{39}Ar)_K$ correction factor of, for example, 0.015 is used instead of 0.001, then model ages in Table 1 and ages reported in Table 2 will decrease by ~13 kyr. Hence ages reported in Table 2 could be systematically older than actual eruption ages. While the large uncertainty on $(^{40}Ar/^{39}Ar)_K$ therefore may affect the apparent age, because this correction is systematic, proposed hiatus durations will not be affected by changing the $(^{40}Ar/^{39}Ar)_K$ correction factor. Uncertainties reported in Table 2 reflect inclusion of analytical uncertainty as well as estimates of uncertainty in J, backgrounds, and the $(^{40}Ar/^{39}Ar)_K$ correction factor.

Feldspar crystals were melted using a 5-W Ar-ion laser. Most sample ages were characterized by 6-12 individual analyses (each analysis aliquot weighed ~10-15 mg). Isotopic measurements were performed using the University of California, Los Angeles (UCLA) VG1200S mass spectrometer operated in the electron multiplier mode with a gain of ~150 relative to the Faraday cup. Mass spectrometer backgrounds (^{40}Ar 0.38-0.58 mV, ^{39}Ar 0.71-1.18 mV, ^{38}Ar 0.11-0.18 mV, ^{37}Ar 0.74-1.23 mV, ^{36}Ar 0.17-0.29 mV) and extraction line blanks (3-6x10^{-16} mol ^{40}Ar) were analyzed prior to the start of each sample. Sensitivity was 2 x 10^{-17} mol/mV during the analyses, and mass discrimination was measured at 0.36%/amu; $^{40}Ar/^{36}Ar$ composition for the atmospheric standard was 290±3 during the analysis period. All relevant isotope data and model ages are presented in Table 1.

Ages for each sample were calculated using the following methodology: (1) Weighted mean ages (using all model ages, Table 1) and isochron ages (calculated from regressions using the technique of *York* [1969]) and associated mean sum of weighted deviates (MSWD) were calculated for each sample. Where 6-12 analyses characterize a single sample age, MSWD of ≤2.0-2.6 represent homogeneous crystal populations [*Wendt and Carl*, 1991]. In both the weighted mean and isochron approaches, 17 samples had MSWD greater than these limits and are therefore apparently characterized by heterogeneous crystal populations. (2) Because of this apparent heterogeneity, a methodology similar to that reported by *Deino and Potts* [1990] and *Spell and Harrison* [1993] was adopted to assess the consequences of excluding analyses that may contribute to the large MSWD. Apparent outliers, which were identified from the isochron regression, were sequentially excluded, and the isochron age and $MSWD_i$ were recalculated. The isochron age was considered "acceptable" when the age and $^{40}Ar/^{36}Ar$ stabilized. With only one exception (91-67), all $MSWD_i$ stabilized at <3.0 (similar to results of *Spell and Harrison* [1993]) after exclusion of 5 to 45% of the analyses. The resulting isochron age, $MSWD_i$ and $^{40}Ar/^{36}Ar_i$ are reported in Table 2. (3) Using the $^{40}Ar/^{36}Ar_i$ composition, an age for each analysis (excluding outliers identified in step 2) was recalculated,

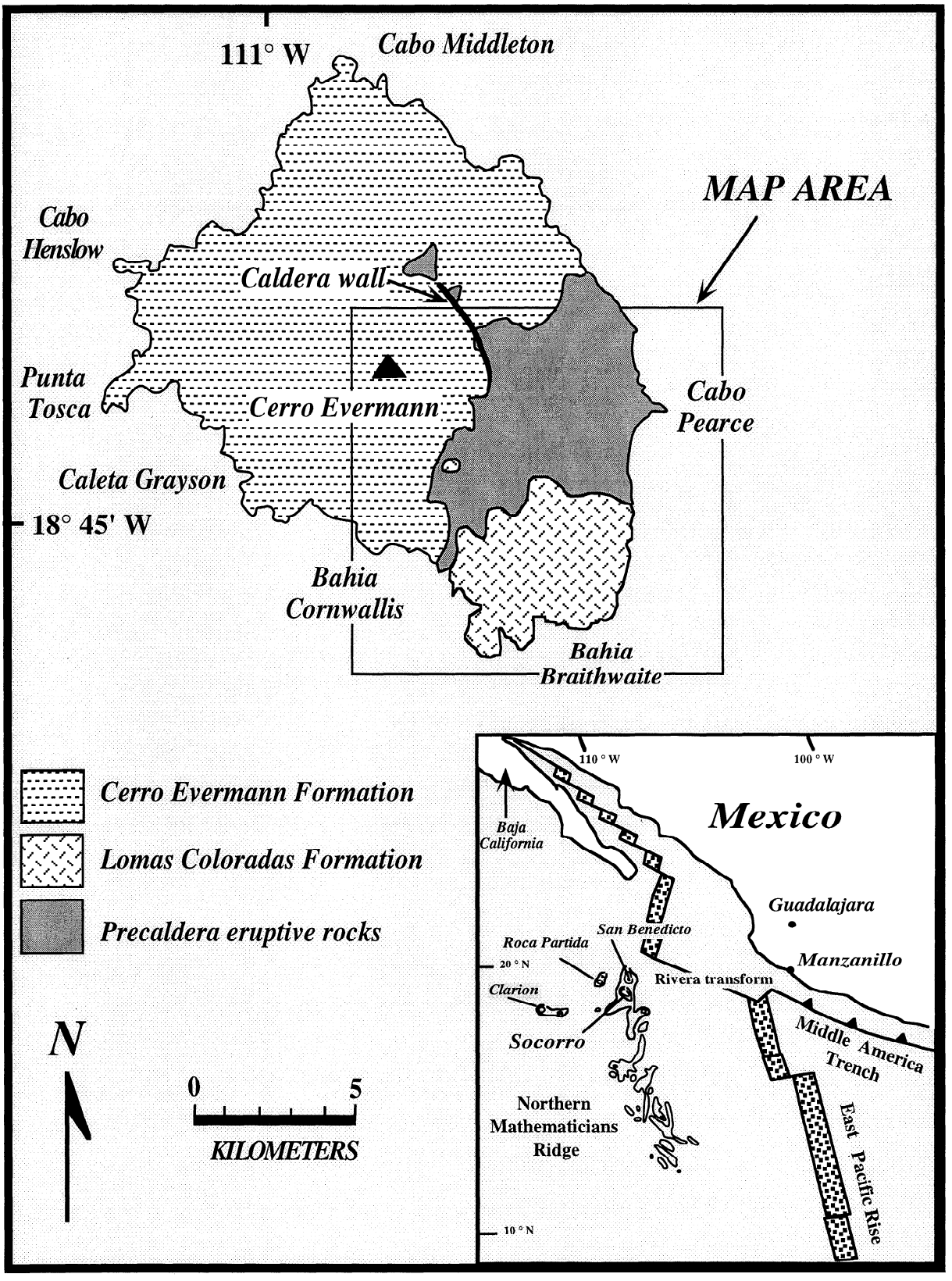

Figure 1. Simplified geologic map of Socorro Island, Mexico, illustrating precaldera and postcaldera phases (Cerro Evermann and Lomas Coloradas Formations) defined by *Bryan* [1959, 1966, 1976]. Place names are included for reference. The box outlines area of Figure 2. The summit, Cerro Evermann, rises to 1050 m. Inset is a tectonic map of the eastern Pacific Ocean modified from *Howell et al.* [1985]. Bathymetric contours show the location of the four Revillagigedo Islands and the northern Mathematicians Ridge.

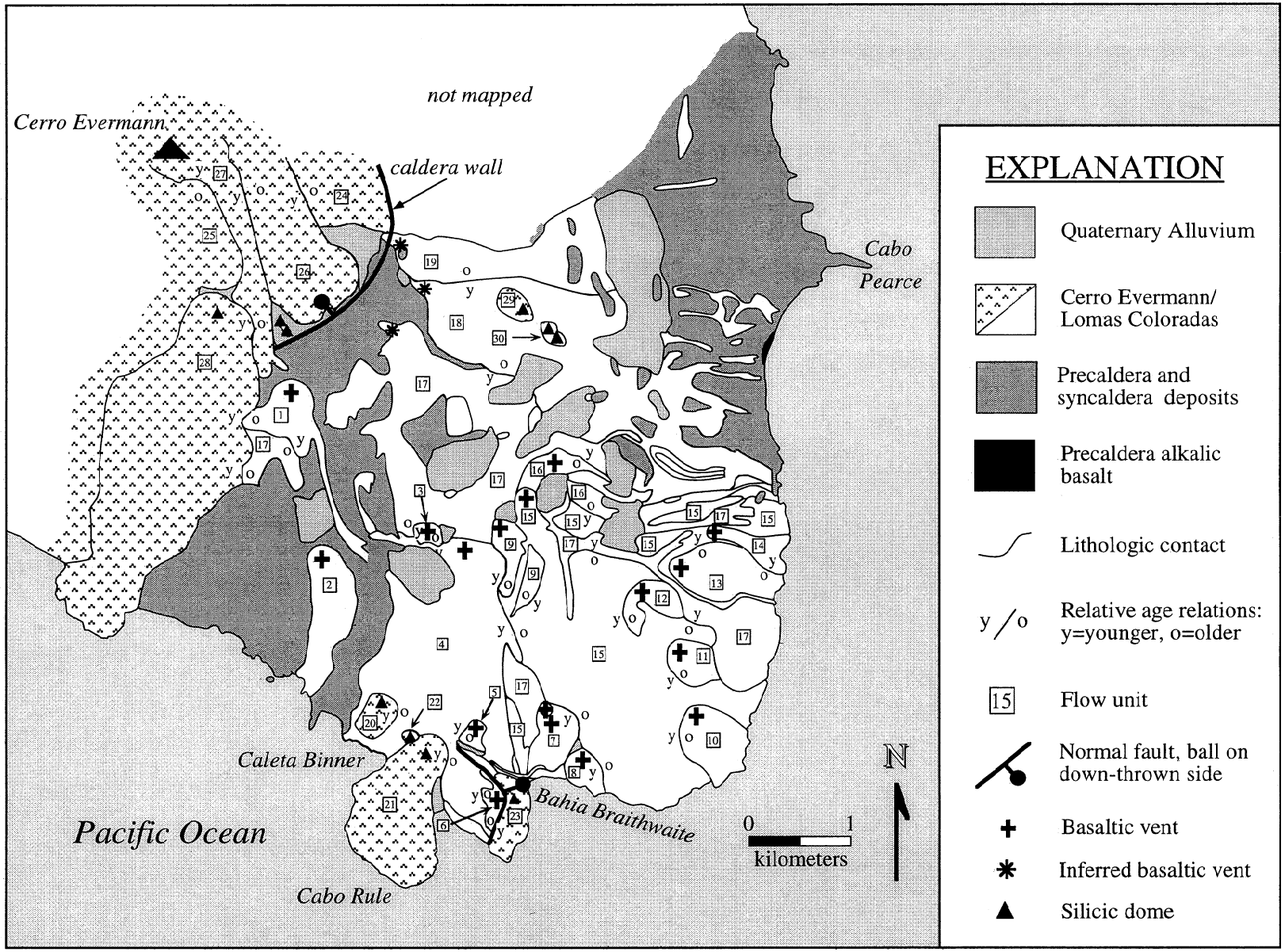

Figure 2. Geologic map of the southeastern quadrant of Socorro Island. Numbers identify individual members of the Cerro Evermann or Lomas Coloradas Formations but do not have stratigraphic significance; in several cases, for clarity, small exposures of previously numbered units were omitted. Where stratigraphic relations were determined in the field, they are labeled with "y/o".

Table 1. The $^{40}Ar/^{39}Ar$ Data

	$^{40}Ar/^{39}Ar^a$	$^{37}Ar/^{39}Ar,^b$ x 10^{-2}	$^{36}Ar/^{39}Ar,^a$ x 10^{-3}	^{39}Ar, x 10^{-14} mol	$^{40}Ar^*$ %	$^{40}Ar^*/^{39}Ar_K$	Age ± 1σ, ka
			90-53 J=0.0004842				
A	1.205	12.75	1.992	3.58	51.5	0.628	548±5
B	1.070	1.742	1.578	3.45	56.0	0.605	528±6
C	1.060	1.540	1.512	3.94	57.5	0.614	537±6
D	1.045	1.409	1.515	3.46	56.7	0.599	523±5
E	1.113	1.026	1.723	3.02	53.7	0.604	527±9
F	1.208	1.562	2.048	3.39	49.3	0.605	528±7
G	1.107	1.964	1.673	3.41	54.7	0.614	537±4
H	1.094	1.744	1.625	3.97	55.5	0.615	537±6
I	1.122	1.775	1.715	3.94	54.3	0.617	538±5
J_1	1.492	2.319	3.022	1.28	39.2	0.601	525±9
J_2	0.971	2.273	1.261	2.80	60.6	0.601	524±7
			91-46 J=0.0004844				
A	1.130	1.871	1.743	2.99	53.7	0.617	539±5
B	1.136	1.871	1.825	3.45	51.8	0.598	522±4
C	1.050	2.026	1.529	4.09	56.3	0.600	524±3
D	1.013	1.807	1.409	3.92	58.3	0.598	522±5
E	1.101	2.294	1.773	3.58	51.9	0.579	506±3
F	1.443	2.361	2.959	3.70	39.2	0.570	498±8
G	1.065	2.434	1.587	3.37	55.2	0.598	522±6
H	1.143	2.366	1.894	3.15	50.5	0.586	512±4
I	1.079	2.523	1.618	3.97	55.3	0.603	527±7
J_2	1.164	1.926	1.943	4.54	50.3	0.591	517±4
			90-13 J=0.0004841				
A	0.906	1.198	0.996	3.93	67.5	0.613	535±4
B	0.922	1.826	1.091	3.73	65.0	0.602	525±4
C	0.993	1.564	1.362	4.16	59.5	0.592	517±5
D	0.934	1.755	1.133	3.54	64.2	0.601	524±4
E	1.005	1.322	1.393	3.86	59.0	0.594	519±5
F	0.964	1.437	1.227	3.48	62.4	0.603	526±4
G	1.057	1.691	1.579	3.36	55.9	0.592	517±4
H	1.020	1.209	1.441	3.76	58.2	0.595	519±6
I	1.018	1.755	1.437	3.62	58.3	0.595	519±6
J_1	1.319	3.771	2.473	0.98	44.6	0.591	516±12
J_2	1.006	1.378	1.376	4.98	59.6	0.601	524±4
			91-67 J=0.0004854				
A	0.827	1.658	0.778	2.81	71.9	0.599	524±3
B	1.029	2.049	1.465	3.30	57.8	0.598	523±3
C	0.851	2.743	0.954	3.64	66.8	0.572	500±4
D	0.885	3.028	1.034	3.69	65.4	0.582	509±4
E	0.833	2.938	0.800	3.80	68.7	0.575	504±2
F	0.853	2.828	0.957	4.61	66.8	0.572	501±4
G	0.939	4.443	1.280	3.56	59.8	0.565	494±3
H	0.879	3.490	1.086	3.57	63.5	0.561	491±6
I	0.878	3.497	1.098	3.90	63.3	0.557	487±5
J_1	1.036	13.05	2.169	1.19	39.2	0.407	356±11
J_2	0.893	5.876	1.296	2.75	57.6	0.515	450±6

Table 1. (continued)

	$^{40}Ar/^{39}Ar^a$	$^{37}Ar/^{39}Ar,^b$ x 10^{-2}	$^{36}Ar/^{39}Ar,^a$ x 10^{-3}	^{39}Ar, x 10^{-14} mol	$^{40}Ar^*$ %	$^{40}Ar^*/^{39}Ar_K$	Age ± 1σ, ka
			90-43B J=0.0004845				
A	0.908	0.251	1.199	3.79	60.1	0.554	484±5
B	0.852	0.813	1.021	4.04	64.1	0.551	481±4
C	0.790	0.633	0.808	3.94	69.2	0.552	482±5
D	0.870	1.080	1.076	3.81	63.0	0.553	483±7
E	0.831	1.306	0.941	4.04	66.1	0.554	484±5
F	0.876	0.012	1.112	3.85	61.7	0.547	478±5
G	1.106	0.675	1.895	3.82	48.9	0.546	477±6
H_1	0.910	0.000	1.218	2.16	59.2	0.550	480±8
H_2	0.782	-0.005	0.759	1.28	68.4	0.558	487±6
I	0.876	0.129	1.127	4.88	61.4	0.543	475±4
			90-76 J=0.0004840				
A	0.894	1.173	1.155	3.27	61.8	0.554	483±5
B	0.905	1.654	1.316	3.78	57.0	0.517	451±4
C	0.892	1.296	1.242	3.91	58.9	0.527	460±3
D	0.861	0.744	1.074	3.69	63.1	0.544	475±3
E	0.882	1.200	1.129	3.47	62.2	0.550	480±3
F	1.220	1.144	2.306	4.03	44.2	0.539	471±4
G	0.887	0.925	1.173	3.62	60.9	0.542	473±4
H	0.952	1.774	1.362	3.72	57.8	0.551	481±6
I	0.980	1.614	1.421	3.07	57.2	0.562	490±5
J_1	1.150	-0.008	2.299	0.65	40.5	0.470	410±10
J_2	0.852	1.715	1.008	3.04	65.0	0.555	485±3
			90-90 J=0.0004831				
A	1.298	1.313	2.732	3.26	37.8	0.492	428±4
B	1.010	2.275	1.753	4.15	48.7	0.494	430±3
C	1.019	2.101	1.772	3.95	48.6	0.497	433±4
D	1.051	1.500	1.858	3.46	47.7	0.503	438±6
E	1.063	2.106	1.910	3.69	46.9	0.501	436±4
F	1.088	1.385	1.990	3.39	45.9	0.501	437±5
G	1.089	1.412	2.026	3.78	45.0	0.491	428±3
H	1.048	1.472	1.883	3.94	46.9	0.493	429±4
I	1.308	1.227	2.789	2.52	36.9	0.485	423±8
J_1	1.494	-0.001	3.309	1.37	34.3	0.517	450±5
J_2	0.941	1.020	1.442	2.40	54.4	0.515	449±4
			90-108 J=0.0004869				
A	1.101	2.280	2.070	3.06	44.3	0.492	432±5
B	1.582	3.053	3.722	2.65	30.5	0.484	425±8
C	1.726	3.042	4.232	1.82	27.5	0.478	420±15
D	1.392	4.991	3.153	2.41	33.2	0.465	408±7
E	1.260	3.121	2.673	2.69	37.3	0.473	416±6
F	1.401	5.776	3.112	2.57	34.5	0.486	427±5
G	1.358	6.574	3.036	2.28	34.1	0.466	409±19
H_1	2.466	22.99	6.805	0.44	19.0	0.475	417±18
H_2	1.040	4.063	1.869	2.82	47.0	0.492	432±6
			91-52 J=0.0004872				
A	0.932	5.079	1.572	1.81	49.5	0.472	415±9
B	0.843	2.372	1.205	3.69	57.6	0.489	429±4
C	1.003	3.218	1.756	3.18	48.1	0.487	427±4

Table 1. (continued)

	$^{40}Ar/^{39}Ar^a$	$^{37}Ar/^{39}Ar,^b$ x 10^{-2}	$^{36}Ar/^{39}Ar,^a$ x 10^{-3}	^{39}Ar, x 10^{-14} mol	$^{40}Ar^*$ %	$^{40}Ar^*/^{39}Ar_K$	Age ± 1σ, ka
			91-52 J=0.0004872 (continued)				
D	0.863	3.998	1.232	2.79	57.7	0.502	441±4
E	0.859	4.838	1.155	3.25	60.3	0.522	458±5
F	0.858	4.648	1.256	3.06	56.7	0.491	431±4
G	0.923	4.060	1.484	2.95	52.4	0.488	428±5
H	0.851	2.745	1.239	2.97	56.8	0.487	428±4
I	0.803	2.234	1.118	3.21	58.6	0.475	417±3
J_1	1.269	8.162	2.727	0.41	35.6	0.470	413±19
J_2	0.753	1.916	0.911	3.89	64.0	0.486	427±2
			91-66 J= 0.0004850				
A	1.073	0.873	2.003	3.19	44.6	0.482	421±3
B	1.138	1.140	2.241	3.37	41.6	0.477	417±5
C	1.349	1.524	2.911	2.78	36.1	0.490	428±9
D	1.169	1.300	2.312	3.65	41.5	0.487	426±3
E	1.218	2.185	2.541	2.77	38.3	0.469	410±6
F	1.250	3.511	2.607	3.15	38.4	0.483	423±7
G	1.094	2.356	2.028	3.73	45.1	0.497	435±4
H	1.197	2.465	2.375	3.23	41.3	0.498	436±7
I	1.373	1.482	3.115	2.11	32.5	0.454	397±8
J_1	1.666	8.258	4.150	0.65	25.9	0.447	390±16
J_2	0.924	0.455	1.520	3.31	51.0	0.475	416±5
			91-64 J=0.0004847				
A	1.165	1.059	2.334	3.11	40.7	0.477	417±9
B	1.516	0.314	3.519	3.14	31.3	0.477	417±7
C_1	3.725	0.443	11.00	1.55	12.7	0.476	416±23
C_2	0.871	-0.015	1.243	2.23	57.1	0.503	439±5
			90-10 J=0.0004840				
A	0.818	1.657	1.249	3.49	54.7	0.450	393±3
B	0.864	1.328	1.458	3.99	50.0	0.435	379±3
C	0.893	1.057	1.542	3.50	48.8	0.438	383±7
D	0.819	0.966	1.279	3.25	53.6	0.442	386±5
E	0.872	1.557	1.478	3.57	49.8	0.437	381±4
F	0.915	0.609	1.615	4.00	47.7	0.438	383±7
G	0.909	1.649	1.530	3.54	50.2	0.458	400±6
H	0.880	1.372	1.331	3.33	55.1	0.488	426±4
I	0.901	1.024	1.580	4.03	48.0	0.435	379±4
J_1	1.668	2.113	2.784	0.74	50.1	0.848	740±23
J_2	1.176	2.094	1.515	2.86	61.8	0.730	638±5
			91-23 J=0.0004869				
A	0.927	0.938	1.701	2.86	45.7	0.425	373±5
B	0.948	0.851	1.747	2.53	45.5	0.433	380±4
C	0.970	2.337	1.819	2.56	44.7	0.435	382±6
D	0.911	1.120	1.633	2.90	47.0	0.430	377±5
E	1.146	0.657	2.456	2.61	36.6	0.421	370±6
F	1.063	0.478	2.149	2.55	40.2	0.429	376±7
G	0.910	0.641	1.665	2.40	45.8	0.418	367±7
H_1	2.804	-0.098	8.322	0.185	11.8	0.337	296±4
H_2	0.768	1.491	1.162	2.53	55.2	0.426	374±5
I_1	1.688	-0.037	4.307	0.46	24.2	0.412	362±21
I_2	0.807	1.197	1.339	2.74	50.9	0.413	362±3

Table 1. (continued)

	$^{40}Ar/^{39}Ar^a$	$^{37}Ar/^{39}Ar,^b$ x 10^{-2}	$^{36}Ar/^{39}Ar,^a$ x 10^{-3}	^{39}Ar, x 10^{-14} mol	$^{40}Ar^*$ %	$^{40}Ar^*/^{39}Ar_K$	Age ± 1σ, ka
			91-23 J=0.0004869 (continued)				
J	1.008	2.934	1.971	3.04	42.3	0.428	376±5
			90-36 J=0.0004840				
A	1.474	1.673	3.521	3.25	29.5	0.435	380±7
B	1.272	1.573	2.860	3.13	33.6	0.428	374±6
C	1.454	1.750	3.490	3.41	29.1	0.424	370±8
D	1.490	1.964	3.610	2.85	28.5	0.425	371±5
E	1.264	2.571	2.841	3.74	33.7	0.427	373±5
F	1.254	1.690	2.803	3.92	34.0	0.428	373±5
G	1.281	2.855	2.884	3.30	33.6	0.432	377±6
H	1.506	2.312	3.690	3.37	27.7	0.417	364±6
I	1.192	2.176	2.605	3.23	35.5	0.424	370±8
J_1	2.026	5.083	5.641	1.10	17.9	0.364	318±22
J_2	0.993	2.688	1.925	2.49	42.8	0.427	373±5
			91-32 J=0.0004842				
A	1.003	0.736	2.007	2.83	40.8	0.410	358±4
B	1.016	0.421	2.029	2.77	40.9	0.417	364±5
C	0.900	1.576	1.583	2.23	48.0	0.433	378±7
D	0.950	0.306	1.747	3.51	45.6	0.434	379±8
E	0.774	4.992	1.188	3.12	55.0	0.427	373±3
F	0.774	-0.002	1.185	2.86	54.5	0.424	370±3
G_1	2.213	-0.002	5.815	0.14	21.9	0.495	432±62
G_2	0.801	0.862	1.284	3.46	52.6	0.422	369±4
H_1	1.295	7.641	3.235	0.49	26.4	0.346	302±22
H_2	0.749	1.180	1.133	4.79	55.3	0.415	362±4
I	0.740	1.920	1.061	3.48	57.6	0.428	374±6
J	0.812	0.0382	1.344	2.93	51.0	0.415	363±5
			91-19 J=0.0004868				
A	0.605	0.500	0.600	3.43	70.4	0.428	376±4
B	0.665	0.195	0.840	3.73	62.4	0.417	366±2
C	0.687	0.442	0.921	3.92	60.2	0.415	364±3
D	0.690	0.158	0.908	3.78	60.9	0.422	370±1
E	0.651	0.772	0.780	3.58	64.5	0.421	370±3
F	0.593	0.032	0.555	3.52	72.1	0.429	377±2
G	0.603	0.549	0.617	3.36	69.6	0.421	370±1
H	0.628	0.409	0.711	3.54	66.3	0.418	367±3
I	0.651	0.877	0.787	3.42	64.2	0.420	369±3
J_1	0.913	-0.623	1.595	0.83	47.8	0.441	387±14
J_2	0.580	0.560	0.522	2.98	73.2	0.426	374±3
K	0.890	0.354	1.598	3.39	46.9	0.418	367±7
L	0.772	1.126	1.224	3.82	53.2	0.412	361±5
M	0.672	0.466	0.869	3.67	62.1	0.422	370±5
N	0.785	0.130	1.236	5.07	53.4	0.419	368±6
			90-95 J=0.0004858				
A	0.946	-0.003	1.790	3.61	43.9	0.417	365±6
B	1.016	-0.004	2.030	3.65	40.8	0.415	364±8
C	0.988	0.801	1.910	3.98	42.9	0.425	372±5
D	1.045	1.498	2.150	3.67	39.3	0.412	361±8
E	1.087	0.331	2.290	4.03	37.8	0.412	361±4
F_1	2.066	-0.034	5.763	0.38	17.3	0.360	316±4

Table 1. (continued)

	$^{40}Ar/^{39}Ar^a$	$^{37}Ar/^{39}Ar$,[b] x 10^{-2}	$^{36}Ar/^{39}Ar$,[a] x 10^{-3}	^{39}Ar, x 10^{-14} mol	$^{40}Ar^*$ %	$^{40}Ar^*/^{39}Ar_K$	Age ± 1σ, ka
			90-95 J=0.0004858 (continued)				
F_2	0.988	1.079	1.912	4.98	42.9	0.424	372±4
F_3	1.165	1.084	2.499	2.98	36.6	0.428	375±4
			91-38 J=0.0004844				
A	2.297	0.509	6.407	3.74	17.5	0.404	353±10
B	2.466	1.678	6.873	3.05	17.6	0.436	381±7
C	9.880	10.60	30.12	0.50	10.0	0.988	863±5
D	1.603	3.021	2.727	2.71	49.7	0.800	699±7
E	3.522	0.634	10.53	3.39	11.6	0.411	359±11
F	2.472	1.418	6.917	2.98	17.3	0.429	375±8
G	3.446	2.972	10.27	3.08	12.0	0.415	363±18
H	2.622	0.640	7.564	3.72	14.7	0.387	338±7
I	2.705	1.543	7.775	3.34	15.1	0.408	357±7
J_1	10.710	9.542	35.16	0.56	3.1	0.330	288±7
J_2	1.175	1.475	2.547	3.66	35.9	0.424	370±6
K_1	8.073	4.070	25.85	1.90	5.4	0.438	382±27
K_2	1.157	2.839	2.501	2.57	36.1	0.420	367±5
			90-115 J=0.0004848				
A	1.225	7.241	2.747	3.32	34.2	0.420	367±5
B	1.158	7.807	2.534	3.11	35.8	0.416	364±7
C	1.090	3.609	2.250	3.33	39.1	0.428	375±6
D	1.104	3.798	2.329	3.51	37.8	0.419	367±5
E	1.198	5.229	2.656	3.11	34.7	0.418	365±6
F	1.226	4.649	2.720	2.81	34.6	0.426	373±7
G_1	2.271	17.49	6.410	0.89	17.1	0.392	343±17
G_2	0.980	3.897	1.879	4.26	43.6	0.429	375±6
H	1.266	7.404	2.807	3.12	34.9	0.443	387±7
I	1.202	5.467	2.651	3.68	35.1	0.423	370±7
J_1	2.031	644.3	11.85	0.98	-44.9	-0.923	-807±306
J_2	0.871	4.119	1.546	4.91	47.8	0.418	365±3
			91-43 J=0.0004848				
A	2.145	-0.001	5.838	3.34	19.5	0.420	367±9
B	2.044	0.610	5.521	3.33	20.2	0.413	361±8
C	2.312	0.570	6.436	3.26	17.8	0.411	359±9
D	2.657	0.209	7.600	2.80	15.5	0.411	360±11
E	2.275	0.970	6.221	3.63	19.2	0.437	382±12
F	2.098	-0.002	5.687	3.66	19.9	0.417	364±6
G	2.196	0.816	6.104	3.21	17.9	0.393	343±10
H	2.102	0.092	5.692	3.30	20.0	0.420	367±7
I	2.083	0.234	5.639	3.36	20.0	0.417	365±10
J_1	5.898	0.450	18.57	0.99	7.0	0.412	360±31
J_2	1.294	1.068	2.966	4.51	32.3	0.418	365±8
			90-41 J=0.0004829				
A	1.349	11.08	3.248	2.01	29.4	0.399	347±12
B	1.140	8.008	2.453	2.78	36.9	0.422	368±7
C	1.202	6.930	2.652	2.39	35.1	0.424	369±8
D	1.164	7.854	2.599	2.24	34.4	0.403	351±10
E	1.062	6.122	2.209	2.97	38.9	0.415	361±6
F_1	1.764	16.92	4.874	0.59	18.9	0.339	295±20
F_2	0.969	8.337	1.956	2.92	40.9	0.399	347±6

Table 1. (continued)

	$^{40}Ar/^{39}Ar^a$	$^{37}Ar/^{39}Ar$,[b] x 10^{-2}	$^{36}Ar/^{39}Ar$,[a] x 10^{-3}	^{39}Ar, x 10^{-14} mol	$^{40}Ar^*$ %	$^{40}Ar^*/^{39}Ar_K$	Age ± 1σ, ka
			90-41 J=0.0004829 (continued)				
G	1.125	8.177	2.405	2.39	37.2	0.422	367±5
H	1.097	8.235	2.402	2.29	35.7	0.395	344±10
I	1.148	12.67	2.550	2.15	35.1	0.405	353±6
J_1	2.035	11.66	5.726	0.73	17.1	0.353	307±14
J_2	1.068	7.487	2.269	3.60	37.7	0.404	352±8
			91-17 J=0.0004860				
A	0.608	1.952	1.358	4.07	32.8	0.209	183±4
B	0.644	1.241	1.532	4.59	29.1	0.192	168±3
C	0.706	1.641	1.608	4.33	32.8	0.233	204±4
D	0.665	0.836	1.557	4.96	30.3	0.206	181±4
E	0.707	0.740	1.759	3.97	25.9	0.188	165±5
F	0.676	1.409	1.578	3.94	30.2	0.211	185±7
G	0.594	1.643	1.334	4.31	33.2	0.201	177±4
H	0.664	1.411	1.511	3.34	31.9	0.218	192±5
I_2	0.653	1.210	1.515	4.92	31.0	0.207	181±6
J_1	2.584	11.81	9.332	0.14	-5.35	-0.163	-143±57
J_2	0.622	0.711	1.429	5.41	31.6	0.200	176±4
K	0.704	1.142	1.728	3.06	27.5	0.194	170±7
L	0.835	0.773	2.123	3.31	24.8	0.208	182±5
M	0.707	0.789	1.718	3.87	28.2	0.200	175±5
N	0.728	0.512	1.800	3.70	27.0	0.197	172±6
			90-94 J=0.0004856				
A	0.638	0.683	1.576	3.81	27.0	0.173	151±4
B	0.562	0.864	1.338	3.46	29.7	0.168	147±3
C	0.605	1.190	1.477	3.28	27.9	0.170	149±4
D	0.587	0.974	1.418	3.40	28.6	0.168	148±9
E	0.664	0.511	1.644	2.64	26.7	0.178	156±5
F	0.617	0.315	1.520	3.25	27.1	0.168	147±6
G	0.598	0.883	1.439	3.51	28.9	0.174	152±4
H	0.647	1.029	1.616	3.37	26.2	0.170	149±4
I	0.640	1.414	1.626	3.91	25.1	0.161	141±6
J_1	0.791	1.408	2.228	1.35	16.8	0.134	117±7
J_2	0.507	0.700	1.147	3.79	33.1	0.168	147±3
			90-98 J=0.0004847				
A	0.668	0.598	1.665	3.08	26.4	0.177	154±5
B	0.725	0.665	1.857	2.90	24.3	0.177	154±9
C	1.811	0.386	2.116	2.82	65.4	1.186	137±5
D	0.715	0.288	1.855	2.53	23.3	0.167	147±7
E	0.740	2.137	1.937	3.27	22.8	0.170	148±3
F	0.939	1.489	2.696	3.25	15.2	0.143	125±6
G	1.235	5.740	3.856	0.41	8.0	0.100	87±14
H	0.716	2.151	1.860	2.96	23.5	0.168	147±4
I_1	1.669	5.939	5.431	0.20	4.1	0.069	61±62
I_2	0.738	1.527	1.954	2.88	21.9	0.162	142±5
J_1	0.875	0.577	2.389	2.78	19.4	0.170	148±7
J_2	0.728	0.553	1.915	3.09	22.3	0.163	142±6
			91-9 J=0.0004863				
A	0.302	0.178	0.719	3.48	29.4	0.090	79±3
B	0.358	0.436	0.938	3.30	22.4	0.081	71±2

Table 1. (continued)

	$^{40}Ar/^{39}Ar^a$	$^{37}Ar/^{39}Ar$,[b] x 10^{-2}	$^{36}Ar/^{39}Ar$,[a] x 10^{-3}	^{39}Ar, x 10^{-14} mol	$^{40}Ar^*$ %	$^{40}Ar^*/^{39}Ar_K$	Age ± 1σ, ka
			91-9 J=0.0004863 (continued)				
C	0.329	0.129	0.826	3.05	25.6	0.085	74±3
D	0.362	0.508	0.959	3.70	21.7	0.079	69±2
E	0.373	1.173	0.934	3.07	26.2	0.099	86±4
F	0.386	0.442	1.038	3.57	20.5	0.080	70±2
G	0.356	0.723	0.922	2.55	23.3	0.084	73±4
H	0.387	-0.005	1.011	3.61	22.6	0.088	77±4
I	0.319	1.119	0.789	3.21	27.1	0.087	76±3
J	0.545	0.184	1.565	3.40	15.1	0.083	72±4
			90-29 J=0.0004837				
A	2.212	4.165	7.285	3.50	2.8	0.063	55±15
B_1	3.207	4.435	10.75	2.06	1.1	0.035	31±15
B_2	0.586	4.097	1.724	5.13	13.6	0.080	69±3
C_1	2.373	4.730	7.851	4.43	2.4	0.058	50±6
C_2	0.541	3.973	1.595	3.38	13.4	0.073	63±4
D	0.546	4.747	1.638	2.80	12.0	0.066	57±5
E_1	2.785	4.438	9.299	4.19	1.5	0.041	35±10
E_2	0.652	3.913	1.966	3.53	11.4	0.074	65±4
F	0.584	3.864	1.730	2.96	13.0	0.076	67±6
G_1	2.202	3.332	7.292	5.46	2.3	0.050	44±11
G_2	0.607	3.060	1.822	2.74	11.7	0.072	62±4
H	0.754	3.184	2.304	2.82	10.0	0.076	66±5
			90-40 J=0.0004845				
A	0.906	1.231	2.814	3.31	8.3	0.076	66±7
B	1.005	0.356	3.186	3.29	6.3	0.064	56±9
C_1	2.981	7.534	10.29	0.27	-1.8	-0.053	-46±47
C_2	0.585	1.330	1.745	2.86	12.0	0.071	62±5
D	0.938	1.990	2.974	2.63	6.5	0.061	53±8
E_1	4.126	1.861	13.98	0.47	-0.99	-0.004	-4±35
E_2	0.666	0.411	2.037	3.27	9.6	0.064	56±4
E_3	0.721	2.048	2.191	3.33	10.4	0.075	66±5
F_1	3.230	6.985	11.01	0.49	-0.54	0.017	-15±37
F_2	0.725	0.835	2.206	5.79	10.2	0.074	65±4
G_1	2.802	3.925	9.399	0.70	1.0	0.028	25±22
G_2	0.658	1.935	1.999	3.26	10.4	0.069	59±7
G_3	0.765	1.056	2.315	3.18	10.7	0.082	71±6
			90-122 J=0.0004835				
A	1.032	5.826	3.294	2.93	6.1	0.064	56±6
B	0.934	6.274	2.920	2.80	8.1	0.077	67±7
C_1	2.117	10.68	7.204	0.43	-0.13	-0.003	-3±23
C_2	0.781	5.958	2.450	2.51	7.7	0.061	53±6
D	1.136	9.579	3.576	3.08	7.7	0.088	76±5
E	1.184	5.296	3.729	2.80	7.3	0.087	76±4
F	0.975	4.997	3.085	3.49	6.9	0.068	59±4
G	1.050	6.055	3.340	3.16	6.5	0.069	60±7
H	1.265	5.034	4.075	2.98	5.1	0.065	56±7
I	1.256	5.080	4.013	2.72	5.9	0.075	65±7
J_1	1.811	10.20	6.123	1.33	0.6	0.010	9±15
J_2	1.004	5.909	3.191	3.66	6.5	0.066	57±5

Table 1. (continued)

	$^{40}Ar/^{39}Ar^a$	$^{37}Ar/^{39}Ar$,[b] x 10^{-2}	$^{36}Ar/^{39}Ar$,[a] x 10^{-3}	^{39}Ar, x 10^{-14} mol	$^{40}Ar^*$ %	$^{40}Ar^*/^{39}Ar_K$	Age ± 1σ, ka
			90-99 J=0.0004828				
A	1.364	0.289	4.465	3.54	3.3	0.045	39±8
B_2	1.272	0.030	4.181	3.61	2.8	0.036	31±6
C_1	3.000	0.394	10.19	1.54	-0.41	-0.012	-11±14
C_2	0.842	0.151	2.637	2.06	7.4	0.062	54±7
D	1.858	0.000	6.134	3.29	2.4	0.045	39±6
E	2.857	0.568	9.353	1.75	3.3	0.094	81±15
F_1	3.739	2.207	12.60	1.35	0.5	0.017	15±22
F_2	6.732	0.271	22.88	2.14	-0.44	-0.030	-26±16
G_1	1.935	0.515	6.421	1.42	1.9	0.038	33±14
G_2	1.102	1.154	3.490	1.36	6.4	0.071	62±9
G_3	0.989	0.201	3.174	0.58	5.1	0.051	44±16
H_1	2.669	-0.005	9.150	2.63	-1.33	-0.036	-31±14
H_2	13.740	4.135	46.28	0.62	0.5	0.068	59±47
I_1	1.514	1.035	4.981	1.97	2.9	0.043	38±6
I_2	0.905	0.563	2.888	1.60	5.8	0.052	46±7
			90-91 J=0.0004836				
A	0.838	5.459	2.809	3.14	1.5	0.013	11±4
B	2.709	5.553	9.152	0.89	0.4	0.010	8±20
C	0.653	5.685	2.172	2.57	2.5	0.016	14±6
D	2.206	6.769	7.665	2.72	-2.43	-0.054	-47±9
E	0.628	5.638	2.103	2.31	1.8	0.011	10±7
F	0.716	5.410	2.377	3.68	2.6	0.018	16±5
G	0.733	5.626	2.479	4.12	0.7	0.005	4±5
H	1.935	6.966	6.699	2.97	-1.99	-0.039	-34±7
I	1.272	6.899	4.371	2.80	-1.07	-0.014	-12±8
J_1	0.616	5.671	2.010	3.09	4.4	0.027	24±6
J_2	0.709	5.050	2.366	3.44	2.0	0.014	12±3
K	1.007	5.801	3.429	3.47	-0.18	-0.002	-2±5

Subscripts denote step-heated samples; e.g., J_1= 2.0-2.5 W step, J_2= 5.0 W step (full melting), analyses with <0.05x10^{-14} mol ^{39}Ar excluded. λ=5.543x10^{-10}yr^{-1} [*Steiger and Jager*, 1977], 1σ uncertainty for model ages reflects analytical uncertainty only; uncertainty in *J* factor, backgrounds, correction factors not included.

[a]corrected for backgrounds and blank.

[b]corrected for ^{37}Ar decay, backgrounds, and blanks.

Table 2. Summary of Supporting $^{40}Ar/^{39}Ar$ and Compositional Data

Sample	Weighted Mean Age ± $1\sigma_{S.E.}$ ($MSWD_w$) [a,b]	*N* Gaussian-like Dist[c]	Mean Age ± $1\sigma_{S.E.}$ [d]	Isochron Age± $1\sigma_{S.D.}$ ($MSWD_i$)	$^{40}Ar/^{36}Ar_i$ ± $1\sigma_{S.D.}$	SiO_2, wt %	Zr, ppm
A							
90-53	534±6 (1.8)	11/11	540±6	526±16 (2.1)	301.0±8.7	65.28	728
91-46	518±5 (4.5)	6/10	528±5	541±11 (0.5)	282.3±5.7	63.31	747
90-13	523±5 (1.5)	11/11	525±6	546±11 (0.9)	275.6±6.0	64.93	759
B (?)							
91-67	501±5 (33.4)	7/11	506±6	524±18 (3.9)	268.6±16.4	65.86	795
C							
90-43B	481±5 (0.6)	10/10	481±5	487±9 (0.6)	285.3±5.6	67.57	1261
90-76	473±5 (13.7)	6/11	479±5	487±9 (2.4)	287.3± 6.0	64.75	747
D							
90-90	434±5 (2.4)	9/11	433±5	441±11 (1.0)	290.0±4.9	65.18	655
90-108	424±5 (1.8)	6/9	432±5	439±13 (1.3)	290.1±4.5	-	-
91-52	430±4 (6.6)	6/11	430±4	426±7 (0.3)	297.7±3.1	65.47	649
91-66	422±5 (3.4)	7/11	425±5	421±18 (2.8)	295.1±8.2	67.19	1202
91-64	429±6 (3.1)	3/4	420±4	417±6 (0.01)	295.4±0.1	67.30	1214
E							
90-10	406±4 (46.8)[e]	6/11	384±5	431±17 (1.0)	257.1±11.3	64.93	656
91-23	372±4 (1.1)	10/12	378±4	356±13 (2.0)	307.2±.7.4	63.71	552
90-36	372±4 (1.0)	10/11	375±4	377±8 (0.5)	293.4±2.4	65.25	552
91-32	368±4 (2.8)	10/12	374±4	379±10 (2.2)	286.7±6.3	66.11	965
91-19	370±4 (1.6)	14/15	372±4	379±7 (2.0)	281.5±7.3	66.22	1353
90-95	368±4 (1.6)	7/8	371±4	361±23 (2.0)	299.2±11.1	67.80	1429
91-38	403±5 (205.4)[e]	9/13	370±6	368±8 (2.0	295.4±1.1	66.85	1469
90-115	369±4 (1.4)	10/12	369±4	358±10 (1.4)	301.3±4.1	65.64	715
91-43	363±5 (0.8)	11/11	368±5	367±11 (0.9)	294.8±1.6	67.07	1477
90-41	356±4 (3.4)	8/12	367±5	378±45 (1.8)	288.2±17.7	65.01	867
Cerro Evermann Formation[f]							
91-17	179±2 (1.2)	12/15	182±3	173±9 (0.7)	300.2±6.1	66.56	829
90-94	148±2 (2.7)	9/11	152±2	125±15 (0.4)	314.5±1.9	66.71	1543
90-98 (#24)	144±2 (4.5)	8/12	150±2	161±21 (0.9)	287.4±10.8	66.58	1631
91-9 (#25)	73±1 (2.8)	7/10	75±1	76±7 (1.3)	289.9±7.4	-	-
90-29 (#20)	62±2 (2.5)	9/12	68±2	69±2 (1.0)	292.9±0.9	64.64	494
90-40	62±2 (94.8)	9/13	66±2	62±15 (1.1)	295.5±5.9	67.70	1471
90-122 (#21)	63±2 (3.2)	8/12	62±2	48±14 (0.5)	299.4±3.8	63.89	465
90-99 (#26)	43±2 (2.2)	9/15	41±4	44±7 (1.6)	295.0±1.3	67.17	1301
90-91 (#28)	12±2 (0.7)	7/12	15±2	17±8 (0.7)	293.7±2.5	64.12	506

[a]All ages and associated uncertainties in ka; weighted mean and mean age uncertainties reflect quadratic combination of analytical uncertainty (1σ S.E.) and 1% uncertainty in *J* (which represents estimated analytical uncertainty in *J* plus estimated uncertainties in backgrounds and $(^{40}Ar/^{39}Ar)_K$); isochron age uncertainty reflects quadratic combination of uncertainty in isochron fit and 1% uncertainty in *J* as noted.

[b]Weighted mean ages and associated $MSWD_w$ include all model ages (Table 1); acceptable $MSWD_w$ should be <2.1 for most samples ($n \geq 8$); the exception is 91-64, which should be <3.7 (n=4).

[c]Indicates fraction of analyses used to calculate mean age, isochron age, $^{40}Ar/^{36}Ar_i$, $MSWD_i$ and associated uncertainties.

[d]Mean age estimated using results of probability density function.

[e]Model age data suggest presence of older xenocrysts. Excluding xenocrysts, recalculated weighted mean age±1σ, ($MSWD_w$), respectively: 90-10 389±4, (10.3); 91-38 364±4, (2.4).

[f]Unit numbers (Figure 2) included in parentheses.

thereby accounting for deviations from atmospheric $^{40}Ar/^{36}Ar$ composition (295.5) assumed in model age calculations (see *McDougall and Harrison* [1988] for discussion). Using these recalculated ages, a probability density function [e.g., *Taylor*, 1982; *Bevington and Robinson*, 1992] was calculated for each sample. In several cases, additional outliers were excluded and steps 2 and 3 were repeated until the probability density function had a Gaussian-like distribution, which is indicative of a homogeneous crystal population [e.g., *Bevington and Robinson*, 1992]. Mean ages identified by the Gaussian-like distributions (hereafter referred to as mean age) along with the fraction of analyses that contribute to it are reported in Table 2. The weighted mean age and the mean age for 25 of 30 samples overlap at $1\sigma_{S.E.}$. Of the five samples that do not overlap, two model ages for each of two samples (90-10 and 91-38) are significantly older than the remaining analyses, suggesting contamination by older xenocrysts.

Geologic History: Mapping and $^{40}Ar/^{39}Ar$ Results

Mapping of the southeastern quadrant of Socorro Island and $^{40}Ar/^{39}Ar$ results support *Bryan's* [1959, 1976] distinction of precaldera and postcaldera phases on Socorro, with the latter comprising two formations, the Cerro Evermann and the Lomas Coloradas; in addition, we tentatively identify a syncaldera eruptive phase. Our map area is outlined in Figure 1, and our geologic map is illustrated in Figure 2. Eruptive

ages of precaldera and syncaldera and Cerro Evermann rocks are constrained by $^{40}Ar/^{39}Ar$ (Table 1) data whereas plagioclase in alkalic basalts of the Lomas Coloradas Formation are not amenable to this technique because of their low $^{40}Ar^*$ yield (<1%) and high Ca/K (49±5).

Precaldera and Syncaldera Phase

The oldest units subaerially exposed on Socorro Island are precaldera basalts and precaldera and syncaldera peralkaline trachytes and rhyolites that are largely confined to the eastern side of the island. Exposure of precaldera basalt is limited to the base of an inaccessible cliff south of Cabo Pearce (Figure 2 and *Bryan* [1959]), where the basalts are overlain by precaldera silicic peralkaline deposits. All precaldera and syncaldera silicic trachytes and rhyolites are phyric (up to 15 vol % total phenocrysts), with alkali feldspar >> Na-pyroxene ≈ fayalite >> aenigmatite. Groundmass is typically composed of alkali feldspar + Na-pyroxene + aenigmatite ± sodic amphibole. The total volume of precaldera and syncaldera silicic peralkaline rock calculated using estimates of average deposit thickness and average area is 2 km^3 (dense rock equivalent) (Table 3); this estimate is a minimum because it does not account for possible deposits in the ocean or those concealed by younger units.

Stratigraphy of precaldera and syncaldera phase based on $^{40}Ar/^{39}Ar$ ages. Twenty-one $^{40}Ar/^{39}Ar$ ages of silicic peralkaline deposits provide evidence for a silicic precaldera and syncaldera eruptive history characterized by several distinct eruptive periods (Figures 3 and 4 and Table 2). Most mean ages cluster at ~430 or ~375 ka, suggesting two distinct eruptive episodes. Six samples yield older mean ages that define two, or possibly three, additional eruptive episodes. The eruptive products of these five periods are informally designated from oldest to youngest as A, B(?), C, D, E. Although in most locations, stratigraphic relations for silicic precaldera and syncaldera deposits could not be determined, those that could be resolved (n=2) are consistent with $^{40}Ar/^{39}Ar$ ages.

Deposits of A-D are unequivocally older than the exposed caldera because they have ages older than those samples that comprise the caldera wall. Two samples of E (90-95 and 91-19) compose the caldera wall, suggesting that E is either precaldera or syncaldera in age; we interpret E as syncaldera, in part, because of the well-documented association between explosive eruptions and caldera formation [*Smith*, 1979].

Rocks of the oldest silicic peralkaline eruptive period sampled (A) range in mean age from 540±6 (90-53) to 525±6 ka (90-13). Consistent with their ages, sample 90-53 lies stratigraphically below 90-13 in a single exposure north of Cabo Pearce. Sample 91-67 yields a mean age of 506±6 ka and is designated B(?). The questionable designation reflects the unacceptable $MSWD_i$ (3.89, Table 2) and the lack of additional samples of similar age. The bimodal probability density function suggests that the crystal population may be heterogeneous (e.g., contains xenocrysts), in which case, the age may have little geologic meaning. C erupted at ~480 ka and is represented by samples collected from near the eastern coast, north of Cabo Pearce. Eruption of C followed a quiescent period of at least 14 kyr since eruption of B(?) and at least 33 kyr since eruption of A. D erupted between 433±5 and 420±4 ka following at least 36 kyr of quiescence and includes samples from both the eastern and southern quadrants. Eruption of E occurred between 384±5 and 367±5 ka, following a minimum of 27 kyr of inactivity; E includes samples from the caldera wall, as well as from the southern and eastern flanks.

Lithofacies description. Silicic peralkaline precaldera and syncaldera deposits on Socorro Island are commonly holocrystalline, nonfragmental, nonvesicular lava-like deposits that lack inclusions or lithic fragments. However, horizons characterized by fiamme and lithic fragments are locally preserved and are typically characterized by well-developed eutaxitic foliation, vitroclastic texture, and between 5% and 20% fiamme in a welded matrix. Fiamme are typically flattened and stretched with the axis of elongation trending downslope. Where exposed in paleostream valleys, the welding zonation parallels paleovalley walls, and fiamme are lineated parallel to the axis of the paleovalley, indicating that rheomorphism may have occurred. Lithic abundances are typically about 10% and include obsidian, vesicular porphyritic basalt, and peralkaline trachyte or rhyolite.

North of Cabo Pearce, A comprises two densely welded zones, each ~15 m thick, that lack both lithic fragments and fiamme (Figure 5); these probably represent distinct cooling units. The lower densely welded zone (90-53), the base of which is not exposed, underlies a breccia composed of subangular peralkaline trachyte and rhyolite clasts set in an ash matrix. A partially welded zone containing partially flattened pumice and angular lithic fragments, overlies the breccia. The upper densely welded zone (90-13) is capped by a partially welded zone. All internal contacts in A are gradational except for those of the breccia. Unit B is densely welded (91-67) throughout except for a 2-m-thick partially welded zone at the top. Partially welded zones associated with C are not observed.

Approximately 1.5 km south of Cabo Pearce, D is distinguished by a complex and thick (1-5 m) basal zone dominated by lithic fragments and pumice. Proportions of lithic fragments and pumice vary, with local concentrations of lithics exceeding 40% and of pumice exceeding 70%. The deposit is clast-supported, with less than 10% ash matrix. In general, it is poorly sorted and massive, although crude stratification defined by size-sorted lithics and fiamme is present in some exposures. Lithic fragments (vesicular basalt and peralkaline trachyte and rhyolite) and pumice range from 0.5 to 50 cm and from <1 cm to rarely >10 cm, respectively. This pumice-lithic rich horizon underlies a densely welded unit (91-64) and grades laterally into a partially welded horizon. In a canyon adjacent to and north of this deposit, partially welded tuff of D grades upsection into a densely welded horizon (91-66).

Twenty five meters of E is exposed in the upper portion of a sea cliff 2 km south of Cabo Pearce. Here, a densely welded layer of E (91-43) overlies A (91-46) and is separated from it by a 1-m-thick ash bed and a 2-m-thick breccia. The ash bed, which directly overlies a densely welded zone of A, is extremely weathered and contains sparse lithics and pumice. The breccia comprises dense, altered, angular silicic peralkaline clasts. The contact between the breccia and E is sharp.

Interpretation of eruptive and depositional processes. Silicic peralkaline magma has relatively low viscosity (compared to metaluminous magmas with similar SiO_2) which can promote dense welding and rheomorphism of

Table 3. Eruption and Growth Rates

	Area,[a] km^2	Average Thickness,[a] m	Volume, km^3	Duration of Volcanism, Ma	Eruption Rate,[b] km^3/yr	Growth rate,[b] km^3/yr
Socorro Island						
Total edifice	-	-	2400	<3.5[c]		>7 x 10^{-4}
Silicic precaldera and syncaldera	30.5[d] (110)	75[e]	2 (8)	0.17	1 x 10^{-5} (5 x 10^{-5})	
Cerro Evermann Formation	77	10	0.8	0.18		
					5 x 10^{-6}	
Lomas Coloradas Formation	21	3	0.1	0.08		
Other volcanoes						
Terceira, Azores[f]	-	-	5.46	0.023	2 x 10^{-4}	
Sao Miguel, Azores[f]	-	-	4.5	0.005	9 x 10^{-4}	
Gran Canaria[f]	-	-	200	0.5	4 x 10^{-4}	
Ascension[g]	-	-	-	1.5	6 ± 3 x 10^{-5}	
Bouvet[g]	-	-	-	0.7	4 ± 1 x 10^{-5}	
Nonhotspot volcano[h]	-	-	-	1-2		1 x 10^{-4}

[a]Area and thickness estimates for Socorro from field data.

[b]Eruption rates for all edifices calculated for subaerial exposures using volume of eruptive phase (estimated using areal extent and average thickness of deposit) and eruption duration. See *Crisp* [1984] and *Gerlach* [1990] for calculation details on edifices other than Socorro; growth rates calculated using duration of volcanism and total edifice volume and therefore may include some intrusive rock.

[c]Maximum age of volcano based on age of underlying oceanic crust. Growth rate is therefore a minimum.

[d]Projected area for precaldera and syncaldera ash flow tuffs estimated on kilometer basis and assumes continuity between exposure of tuffs in SE quadrant; estimate in parentheses is total area of Socorro Island and assumes that tuff mantles entire island. Volume and eruption rate in parentheses use this area estimate.

[e]Sum of thicknesses of several ash flow tuffs from exposures in coastal cliff.

[f]*Crisp* [1984].

[g]*Gerlach* [1990].

[h]*Batiza* [1982].

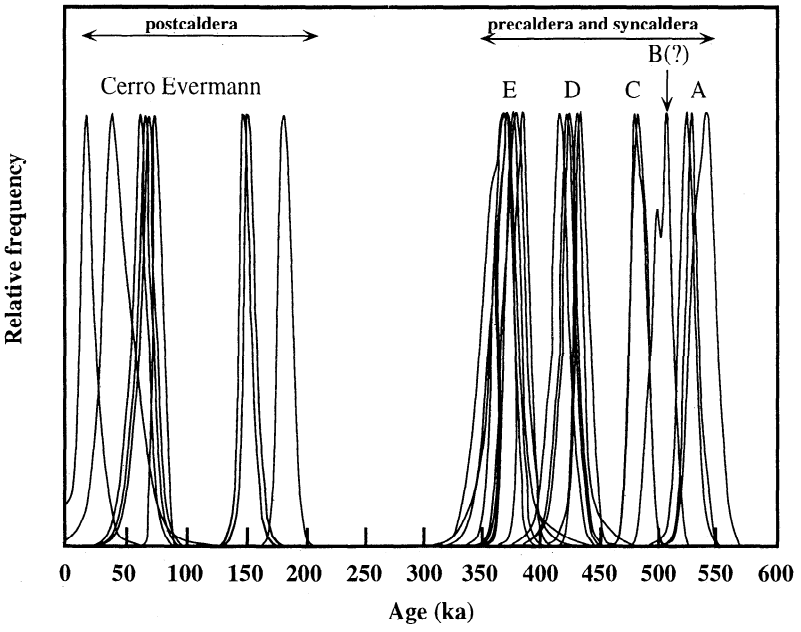

Figure 3. Probability density functions for $^{40}Ar/^{39}Ar$ ages for 30 samples are Gaussian-like, suggesting that the associated samples are characterized by a homogeneous crystal populations. The density functions are typically defined by 6 to 12 individual analyses. Four well-defined, discrete eruptive episodes, which produced precaldera and syncaldera deposits designated A, C, D, and E, range in age from ~540 to 370 ka. One sample (91-67) does not have a Gaussian-like distribution. Instead, the density function is bimodal, which may reflect a heterogeneous crystal population, and hence the associated deposit is designated B(?). Silicic peralkaline postcaldera volcanism, the Cerro Evermann Formation, initiated at ~180 ka after up to 200 kyr of quiescence and continued to at least 15 ka.

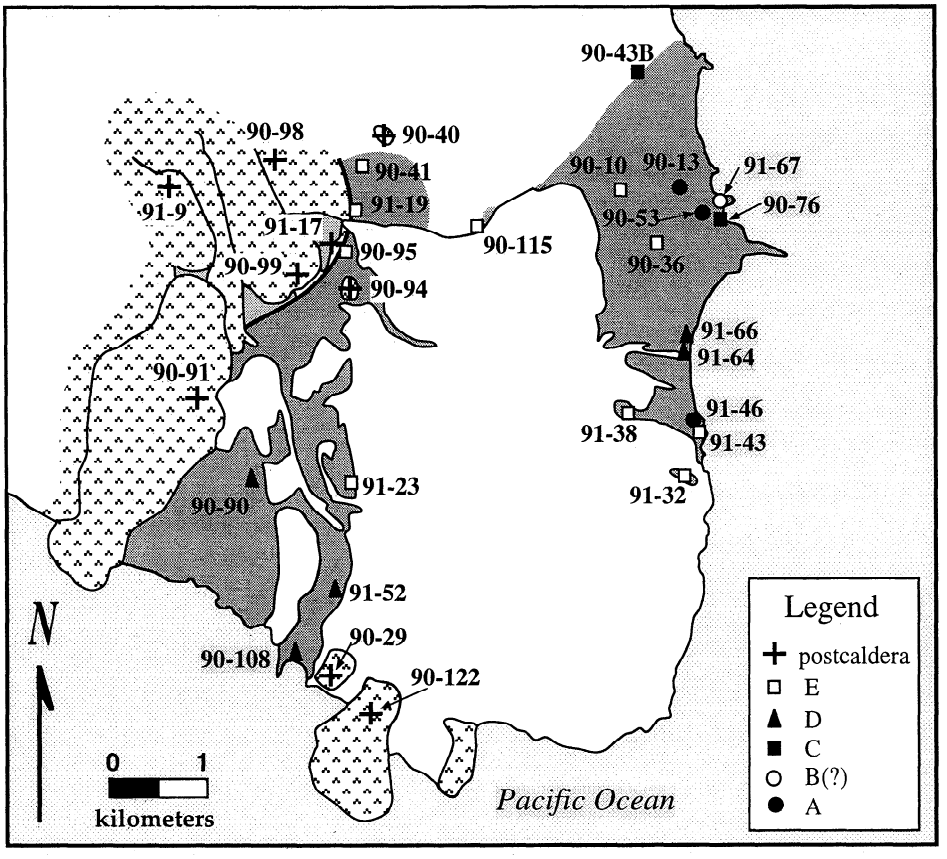

Figure 4. Location map for $^{40}Ar/^{39}Ar$ analyses shows geographic distribution of samples for precaldera and syncaldera deposits and the Cerro Evermann Formation.

pyroclastic deposits [e.g., *Mahood*, 1984]; consequently, silicic peralkaline pyroclastic deposits and extensive lava flows can resemble one another [cf. *Henry and Wolff*, 1992]. Welding zonation such as that described in the previous section is not found in extensive silicic lava flows [e.g., *Henry and Wolff*, 1992] and indicates that many of the precaldera and syncaldera silicic peralkaline deposits on Socorro Island are ash flow tuffs. Other evidence which supports an explosive origin for many of these deposits includes (1) eutaxitic foliation and vitroclastic texture in partially welded zones, (2) broken phenocrysts in some deposits, (3) compositional heterogeneity within a single unit (e.g., D, E, Figure 6) which is more common in ash flow tuffs than lava flows [*Henry and Wolff*, 1992], and (4) tentative association of E with caldera formation.

Further evidence that explosive eruptions dominate the silicic precaldera and syncaldera phase on Socorro is tied to the origin of the lithic-pumice rich horizon associated with D. Characteristics of this zone, including abundant lithic fragments and pumice and a lack of fine particles, are consistent with those described for coarse proximal ignimbrite or co-ignimbrite facies [*Walker*, 1985]. On the basis of the lack of fine particles, the deposit is either a ground layer or a lag breccia (see *Sparks et al.* [1973], *Druitt and Sparks* [1982], and *Walker* [1985] for descriptions of lag deposit and ground layer). Although it can be difficult to distinguish between these deposits [*Walker*, 1985], characteristics of the deposit on Socorro (including thickness, internal stratification, and intimate but irregular association with the ignimbrite) favor the interpretation that the zone is a lag deposit. The significance of this deposit lies less with its exact origin than with its identification as a proximal ignimbrite or co-ignimbrite facies: such deposits have explosive origins, and similar deposits have not been observed with silicic lava flows.

Broken phenocrysts, which are common in pyroclastic deposits, are only moderately abundant in ash flow tuffs from Socorro Island, suggesting that although the eruptions were explosive, the eruption columns may have been low, and fragmentation was not extreme. This is consistent with lower column heights hypothesized for silicic peralkaline eruptions [*Mahood*, 1984] and with the lack of recovery of silicic peralkaline ash in near-by Deep Sea Drilling Project (DSDP) holes [*Shipboard Party*, 1982a, b; *Schmincke*, 1983].

The Caldera

At approximately 600 m elevation on the southeastern side of the summit of Socorro Island, a steep, well-defined, arcuate escarpment forms the eastern boundary of an alluvium-filled depression (Figure 2). This prominent topographic feature is probably the remnant of a caldera wall [*Bryan*, 1959]. Only about 30% of the caldera wall is presently exposed. Using the trajectory of this exposure and the 600-m contour as guides, the reconstructed caldera is ~4.5 x 3.8 km and is elongated NW-SE; such a size is consistent with typical caldera dimensions for peralkaline volcanoes [*Mahood*, 1984]. The best exposure of the wall, which bounds a triangular area of caldera-filling alluvium (caldera floor) defined by two postcaldera lava flows (flows 24 and 26, Figure 2), has more than 30 m of relief, consistent with tens to hundreds of meters of throw that characterize other calderas associated with silicic peralkaline volcanic centers [*Mahood*, 1984]. The western half of the caldera wall is not exposed; *Bryan* [1966] suggested that burial of this section beneath postcaldera flows may have been facilitated by downfaulting along an approximately north-south trending fault, but field evidence for such a fault is absent.

Although nested calderas have been reported for a number of peralkaline edifices (e.g., Pantelleria, Aden, Gariboldi [*Mahood*, 1984]; Mayor Island [*Houghton et al.*, 1992]; Terceira [*Self*, 1976]), structural evidence for nested calderas is absent or covered on Socorro Island, perhaps suggesting that caldera formation did not occur with each of the explosive eruptions. Subhorizontal platy jointing and poorly developed mineral lineation in the caldera wall indicate that the deposit which forms the caldera wall flowed outward from its source prior to caldera formation and was not plastered on an older caldera wall; thus the age of the samples composing the caldera wall are equal to or older than the age of caldera formation. Formation of the caldera therefore occurred between ~370 and 182 ka based on mean ages of the caldera wall and caldera floor, respectively. If the caldera formed at ~370 ka, then collapse may have accompanied eruption of E, which is consistent with the association between caldera formation and explosive eruptions [*Smith*, 1979]. If caldera formation occurred after eruption of E, then collapse may have been triggered by lateral migration of magma or by withdrawal of magma at depth [e.g., *Bryan*, 1966; *Mahood*, 1984], both of which would remove roof support.

Postcaldera Phase

Eruption of E and possible associated caldera formation were apparently followed by up to 200 kyr of volcanic quiescence. Postcaldera silicic peralkaline volcanism, which formed the Cerro Evermann Formation, initiated by ~180 ka and continued until at least 15 ka. Alkaline basalts of the Lomas Coloradas Formation are also postcaldera in age based upon stratigraphic relations.

Cerro Evermann Formation. The Cerro Evermann Formation, which covers ~70% of the island and has a total volume of ~0.8 km^3 (Table 3), includes peralkaline trachytes and rhyolites that erupted in the caldera as well as on the northern, western, and southern flanks (Figures 1 and 2). It is dominated by lava domes, cones, and flows. Scarce evidence of minor explosive activity occurs as thin layers of silicic pumice fallout that are preserved in soils and sediments associated with some vents of the Lomas Coloradas Formation. The phenocryst assemblage for deposits of the Cerro Evermann Formation is alkali feldspar >> Na-pyroxene > fayalite ≈ aenigmatite. Groundmass comprises alkali feldspar + Na-pyroxene + aenigmatite ± glass ± Na-amphibole. Lithologic descriptions presented here draw primarily on observations made in the map area but are supplemented by reconnaissance work to the north and west. Additional descriptions are presented by *Bryan* [1959, 1966].

The oldest recovered sample (91-17, peralkaline rhyolite) of the Cerro Evermann Formation erupted at 182±3 ka and is part of the caldera floor. A glassy, vesicular peralkaline rhyolite lava flow (90-94) with a mean age of 152±2 ka is located to the southeast of the caldera wall, although the source for this flow was not identified. An intracaldera peralkaline rhyolite dome (90-98, flow 24) erupted at 150±2 ka and was confined by the caldera wall to the east. Summit activity at 75±1 ka produced a dome and flow (91-9, flow 25)

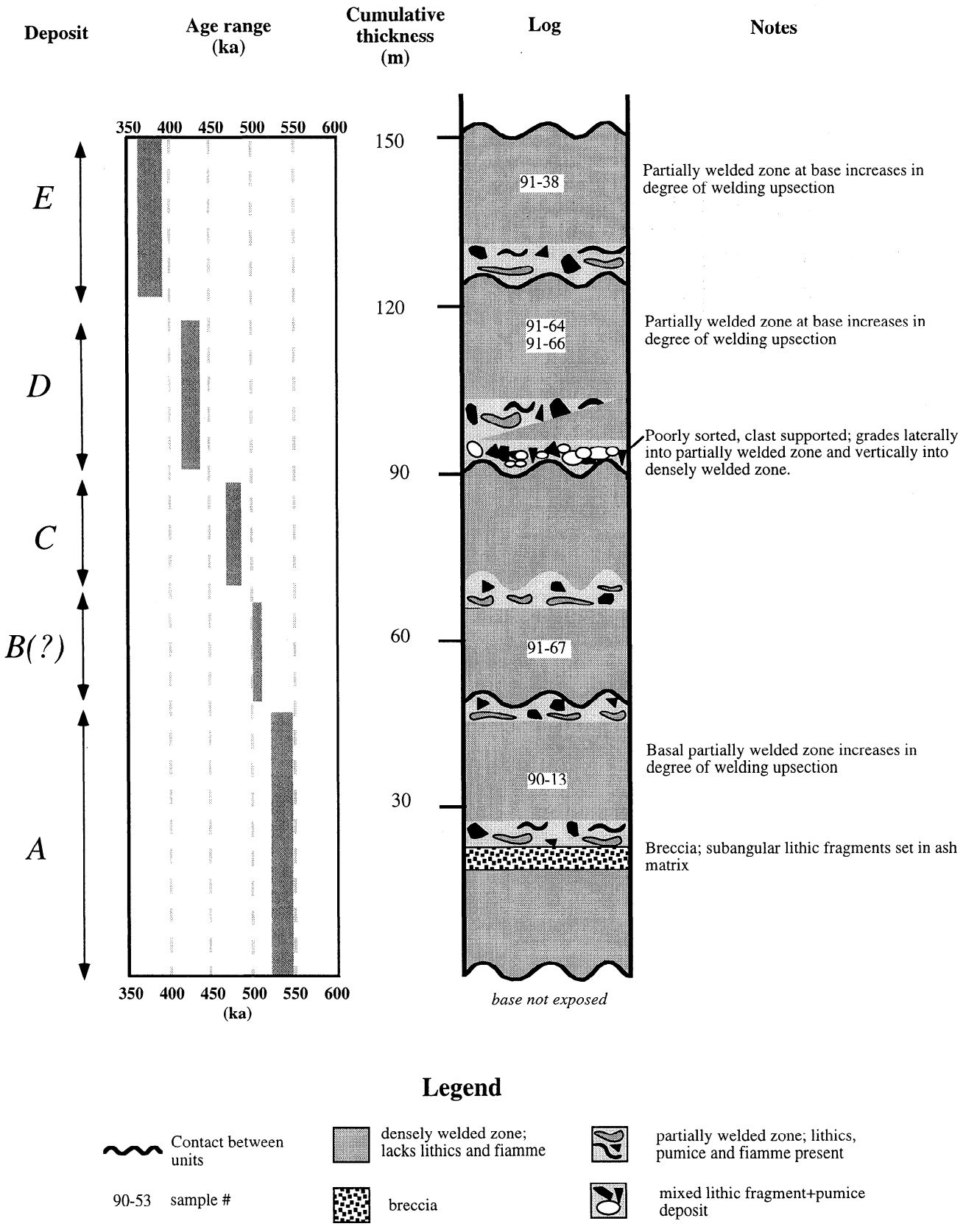

Figure 5. Schematic composite stratigraphic column summarizing age range, welding zonation, and typical thickness for precaldera and syncaldera ash flow tuffs. Age ranges for samples associated with each eruptive episode shown by shaded area. Numbers included in the column represent samples of densely welded tuff taken at or near the location where partially welded deposits were identified. Two densely welded zones separated by a breccia were identified in A; the upper and lower boundaries of the breccia are defined by horizontal black lines. Welding zonation observed for A, B(?), D, and E provides evidence that these deposits are ash flow tuffs rather than lava flows as originally proposed by *Bryan* [1966].

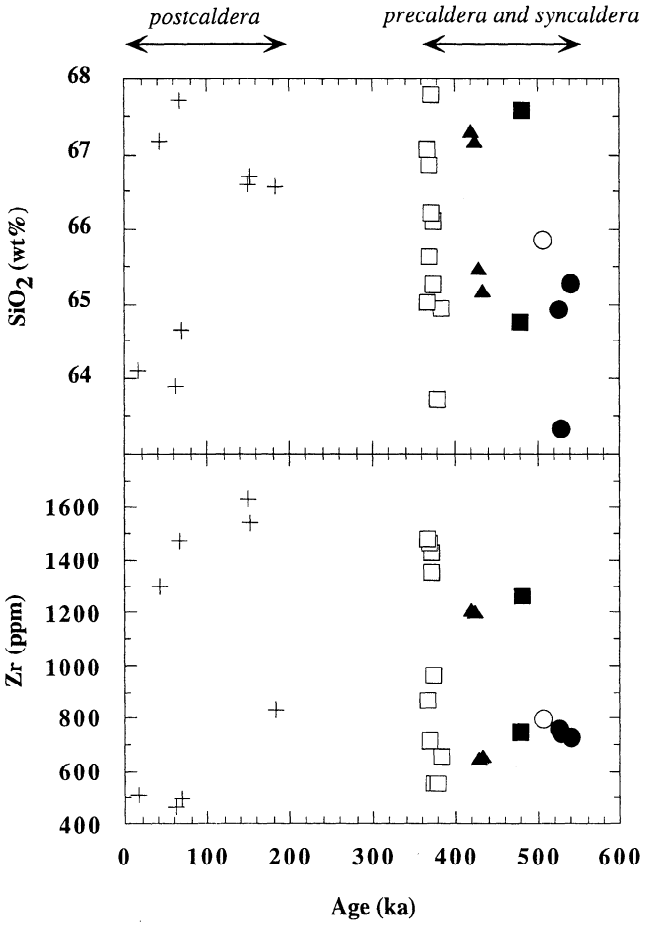

Figure 6. Range of SiO_2 (wt %) and Zr (ppm) for silicic peralkaline rocks from Socorro Island plotted as a function of age. Zr is illustrated because it is one of the most incompatible elements in silicic peralkaline magmas [e.g., *Mahood and Stimac*, 1990]. Individual precaldera and syncaldera deposits are compositionally heterogeneous, a characteristics more common among pyroclastic deposits than extensive silicic lava flows. Collectively, postcaldera domes and flows exhibit compositionally heterogeneity and share similar compositional ranges with precaldera and syncaldera deposits. Symbols are the same as Figure 4. Age uncertainties are smaller than symbol size.

with a pumiceous carapace. A glassy peralkaline rhyolite dome and flow (90-99, flow 26) which erupted at 41±4 ka was apparently confined in the caldera by the caldera wall to the southeast. A peralkaline rhyolite obsidian dome and flow (flow 27) erupted near the summit after 41 ka but before ~15 ka based on stratigraphic relations. At 15±2 ka, an eruption was initiated at about 700 m elevation within the caldera and produced a peralkaline trachyte dome and a lava flow (90-91, flow 28) that traveled 4 km southward into the ocean.

Three peralkaline trachyte domes and a peralkaline trachyte cinder cone originally included in the Lomas Coloradas Formation by *Bryan* [1976] erupted near the southeastern coast between 60 and 70 ka. Because of their silicic peralkaline composition, we include them here in the Cerro Evermann Formation. One dome (90-29, flow 20) and the cinder cone (90-122, flow 21) erupted at 68±6 and 62±5 ka, respectively. Because of the lithologic and compositional similarities between these units and the two undated domes (flows 22 and 23), we suggest they all probably have similar eruption ages.

Lomas Coloradas Formation. The Lomas Coloradas Formation, which covers about 20% of the island and has an estimated volume of 0.1 km^3, comprises alkaline basalt cones and lava flows that are largely restricted to the southeastern quadrant of the island. Seventeen basaltic cinder to spatter cones were identified (Figure 2). Vents could not be identified for three large volume, well preserved flows (flows 17, 18, and 19, Figure 2) indicating that little explosive material was left at their sources. Lava flow morphologies are mainly pahoehoe, with locally well-developed lava tube systems, whereas a'a is subordinate. Total phenocryst abundances range from 0 to 35 vol %, with plagioclase >> olivine ≈ clinopyroxene. Groundmass is composed of plagioclase + olivine + clinopyroxene + Fe-Ti oxides.

All contacts between basalt and precaldera and syncaldera deposits demonstrate that the basalts are younger. One of the oldest basalts (flow 19) overlies a ~150 ka old Cerro Evermann flow, indicating that most of the rocks of the Lomas Coloradas are probably younger than 150 ka. Postcaldera coastal domes and cones of the Cerro Evermann Formation (flows 20 and 21), dated at ~70 ka, postdate one of the younger basalt flows (flow 4), based upon the following observations: (1) in a stream drainage, a trachyte dome (flow 20) overlies the basalt lava flow, (2) basaltic lithic fragments are present in these domes, and (3) the basalt was deformed by intrusion of trachyte (flow 23). Thus the dominant volume of basalt probably erupted between 150 and 70 ka, demonstrating the Lomas Coloradas and Cerro Evermann Formations erupted contemporaneously. At least one episode of basaltic activity postdates the 70 ka old trachyte cones as illustrated by a radiocarbon age of 5040±460 years for lacustrine deposits stratigraphically underlying a volcanic cone (flow 7) located near the southern coast [*Farmer et al.*, 1993].

Stratigraphic relations among the basaltic flows and cones of the Lomas Coloradas Formation were deciphered in most cases using outcrops in stream beds or crosscutting relationships established by dikes (Figure 2; "y/o"). No systematic temporal progression in the distribution of vents and no well-developed, large-scale rift systems are discernible. Where two or more basaltic units could be observed in contact, they were only rarely separated by soils, indicating that the time between basaltic eruptions was probably fairly short.

Discussion

Eruptive Periodicity

The clustering of $^{40}Ar/^{39}Ar$ ages of precaldera and syncaldera deposits from Socorro (Figure 3) implies a periodicity to these eruptions, with eruptive hiatuses of ~30 ka. It has not been possible to confirm the absence of eruptions during these hiatuses because of the difficulty of establishing a stratigraphic framework in the field. However, similarities in apparent hiatus duration despite sampling that covered a wide geographic and elevation range suggest to us that the hiatuses probably have geologic meaning. In the limiting case, the ~30 ka repose periods must be viewed as maxima.

Reference to other silicic peralkaline systems shows that episodic explosive activity and repose periods of 10^4 years are typical. For example, over the last 190 kyr, Pantelleria has

had a silicic eruption every 13±6 ka [*Mahood and Hildreth*, 1986]; among these, many were explosive. The Mogan Formation, Gran Canaria, which is dominated by silicic peralkaline pyroclastic deposits, is characterized by repose periods of 30-50 kyr [*Bogaard et al.*, 1988; *Clark and Spera*, 1990]. The 130 kyr subaerial history of Mayor Island, which comprises intercalated lava and pyroclastic flows, is typified by average repose periods of ~4 kyr [*Houghton et al.*, 1992]. In general, the small eruptive volumes and the short repose times for many peralkaline volcanoes probably reflect small to medium volume magmatic systems [*Spera and Crisp*, 1981; *Bogaard et al.*, 1988; *Houghton et al.*, 1992].

Magma Plumbing System

The presence of a small summit caldera on Socorro suggests that the silicic magma reservoir was shallow [e.g., *Mahood*, 1984], probably located within the volcanic edifice or the upper oceanic crust. This is also supported by phase equilibria for both precaldera and syncaldera and postcaldera silicic peralkaline rocks (W. A. Bohrson and M. R. Reid, manuscript in preparation, 1996). In order to maintain a long history of silicic peralkaline activity, mafic recharge probably maintained thermal viability of the magma reservoir. As a comparison, complete crystallization of the Skaergaard Intrusion (modeled as a single pulse of basaltic magma 3 times larger than that estimated for the chamber associated with Socorro intruded at a depth of 4 km, which is probably equal to or greater than the depth of the chamber associated with Socorro) occurred in 130 ka [*Norton and Taylor*, 1979; *Norton et al.*, 1984]. Evidence for low pressure differentiation for postcaldera basaltic rocks [*Bohrson and Reid*, 1995] coupled with the observation that postcaldera basaltic and silicic eruptions on Socorro were contemporaneous support the inference that basaltic and silicic magma coexisted at shallow levels [cf. *Bryan*, 1966].

Precaldera and syncaldera silicic peralkaline ash flow tuffs are compositionally heterogeneous, as are domes and flows of the Cerro Evermann Formation; in fact, the two phases of activity share similar ranges of compositions as indicated by SiO_2 and Zr (Table 2 and Figure 6). Given the lack of stratigraphic control in the field and the uncertainties in the Ar data, it is not possible to determine whether the ash flow tuffs are vertically compositionally zoned, and thus, whether the silicic magma chamber was itself compositionally zoned or whether compositional heterogeneity within the tuffs reflects a process such as magma mixing. In any case, the transition from explosive to more effusive eruptive style following caldera formation on Socorro suggests an associated change in the magma plumbing system. Factors which control explosivity (changes in magma viscosity, vesiculation depth [*Fisher and Schmincke*, 1984], or parameters of magma ascent [*Eichelberger*, 1995]) were probably more strongly influenced by volatile abundance and type or the degassing history of the magma than by changes in chamber depth or magma bulk composition from the precaldera and syncaldera to postcaldera phases. *Lowenstern and Mahood* [1991] demonstrated that preeruptive volatile abundances of silicic peralkaline magmas from Pantelleria correlate poorly with explosivity and suggested that the decompression history of the magma constitutes the critical element in determining eruption style. On Socorro, ring fractures produced during caldera formation may have facilitated degassing for postcaldera magma. A slower ascent rate for postcaldera magma may have also permitted degassing, thereby producing effusive eruptions, whereas a faster ascent rate for precaldera and syncaldera magmas may have inhibited degassing, thereby producing explosive eruptions [cf. *Eichelberger*, 1995].

Eruption Rates and Possible Source of Magmatism

Calculated eruption rates for Socorro Island decrease with time (Table 3); rates of 4×10^{-6} km^3/yr for the Cerro Evermann Formation and of 1×10^{-6} km^3/yr for the Lomas Coloradas Formation are collectively half that estimated for the precaldera and syncaldera phase (10^{-5} km^3/yr). Similar decreases in eruption rates have been noted for other volcanic edifices (e.g., Hawaii [*Clague*, 1987] and Gran Canaria [*Bogaard et al.*, 1988]). Calculating an eruption rate for the submarine part of the edifice is difficult due to uncertainties in the age of inception of volcanism and an accurate assessment of the intrusive to extrusive ratio. A minimum growth rate of $>7 \times 10^{-4}$ km^3/yr for the edifice, delimited by a ~3.5 Ma age of the underlying ocean crust and a total edifice volume of 2400 km^3, represents primarily submarine growth because the subaerial volume of the volcano (~40 km^3) is <2% of the total edifice volume. Even given the uncertainties noted above, the greater than order of magnitude difference between this growth rate and subaerial eruption rates suggest that either subaerial eruption rates are less than submarine ones or that the growth of the volcano has continued to be dominantly submarine.

Growth and eruption rates permit comparisons of possible sources for different volcanic edifices (Table 3). Growth rates for nonhotspot off-ridge volcanoes [*Batiza*, 1982] are almost an order of magnitude less than that of Socorro, suggesting that magmatism associated with Socorro is probably not solely the product of residual mantle upwelling associated with ridge abandonment. Although eruption rates for ocean island chains such as the Canary Islands are higher than those of Socorro (Table 3), isolated ocean islands thought to be associated with mantle plumes (e.g., Bouvet and Ascension [*Gerlach*, 1990]) have similar subaerial eruption rates to those of Socorro. On the basis of these comparisons, we suggest that the source of alkaline magmatism associated with Socorro may be consistent with a mantle plume [cf. *Duncan and Richards*, 1991]

Conclusions

1. Precise, replicate $^{40}Ar/^{39}Ar$ analyses and relative stratigraphy reveal 0.5 Myr of alkaline and peralkaline volcanism on Socorro Island, a volcanic edifice located on a mid-ocean ridge spreading center abandoned at ~3.5 Ma. The oldest dated rocks, which range in age from ~540 to 370 ka, are precaldera and syncaldera silicic peralkaline ash flows formed by several distinct periods of explosive activity; repose periods between these explosive episodes may have had maximum durations of ~30 kyr. Formation of a small summit caldera occurred during or after eruption of the youngest ash flow tuff. The ~200 kyr hiatus that followed caldera formation ended with postcaldera silicic peralkaline activity (Cerro Evermann Formation) that commenced at ~180 ka and continued to at least 15 ka. Postcaldera alkaline basalts (Lomas Coloradas Formation) erupted between 150 and 70 ka, demonstrating that contemporaneous eruption of silicic and basaltic magmas occurred on Socorro Island.

2. Precaldera and syncaldera deposits are dominantly densely welded ash flow tuffs. Although these deposits resemble lava flows, the presence of welding zonation, a co-ignimbrite or proximal ignimbrite deposit, association with a caldera, and compositional heterogeneity within single eruptive units provide evidence that the deposits are pyroclastic.

3. The magma reservoir beneath Socorro is inferred to reside at shallow depths, probably in the ocean crust or within the volcanic edifice. The shallow depth of the magma chamber coupled with the prolonged history of silicic peralkaline magmatism during both precaldera and syncaldera and postcaldera phases are used to infer that intrusion of basaltic magma maintained thermal viability of the magma reservoir. This requirement coupled with contemporaneous eruption of postcaldera silicic and basaltic magma may be consistent with coexistence of mafic and silicic magma at shallow levels.

4. The short repose periods, small volume eruptions, small caldera and shallow level magma chamber that characterize Socorro Island are similar to those of peralkaline volcanoes located on continental crust (e.g., Pantelleria and Mayor Island), indicating that these features may be independent of crustal structure.

5. Eruption rates for Socorro Island probably decrease with time. Socorro's total growth rate exceeds those of nonhotspot off-ridge volcanoes [*Batiza*, 1982], whereas its subaerial eruption rates are similar to those of isolated ocean islands [*Gerlach*, 1990] where mantle plumes are proposed sources.

Acknowledgments. Field expenses were defrayed by grants from the Geological Society of America and UCLA Program on Mexico (to W. A. B). Other aspects of this study were supported by National Science Foundation grants EAR89-17204 and EAR92-05807 (to M. R. R). We thank Enrique Carballido Sanchez, Jack Farmer, Todd Feeley, Adriana Guzman de la Campa, Michael McGrady, and James Sample for assistance with field work. We also thank Maria Farmer for her invaluable assistance in negotiating for permission to work on Socorro Island and Wilfred Bryan for kindly providing advice on the project. Bohrson especially thanks Gustavo Calderon Riveroll for his generous assistance in obtaining permission to work on Socorro Island and Ricardo Mendoza Anzo, the Mexican Navy, and the people of Socorro Island for their support. Discussions with Keith Mahon and Marty Grove are greatly appreciated as are helpful comments by R. Batiza, G. Mahood, J. McPhie, R. Stevenson, J. White, and J. Wolff. Reviews by W. Bryan, A. Deino, K. Foland, I. McDougall, and M. Streck greatly improved the manuscript.

References

Batiza, R., Abundances, distribution and sizes of volcanoes in the Pacific Ocean and implications for the origin of non-hotspot volcanoes, *Earth Planet. Sci. Lett.*, *60*, 195-206, 1982.

Batiza, R., and D. A. Vanko, Petrologic evolution of large failed rifts in the eastern Pacific: Petrology of volcanic and plutonic rocks from the Mathematician ridge area and the Guadalupe trough, *J. Petrol.*, *26*, 564-602, 1985.

Bevington, P. R., and D. K. Robinson, *Data Reduction and Error Analysis for the Physical Sciences*, 328 pp., McGraw-Hill, New York, 1992.

Bogaard, P., H.-U. Schmincke, and A. Freundt, Eruption ages and magma supply rates during the Miocene evolution of Gran Canaria, *Naturwissen*, *75*, 616-617, 1988.

Bohrson, W. A., and M. R. Reid, Petrogenesis of alkaline basalts from Socorro Island, Mexico: Trace element evidence for contamination of ocean island basalt in the shallow ocean crust, *J. Geophys. Res.*, *100*, 24,555-24,576, 1995.

Bryan, W. B., High-silica lavas of Clarion and Socorro Island, Mexico--Their genesis and regional significance, Ph.D. thesis, 164 pp., Univ. of Wis.-Madison, 1959.

Bryan, W. B., History and mechanism of eruption of soda-rhyolite and alkali basalt, Socorro Island, Mexico, *Bull. Volcanol.*, *29*, 453-479, 1966.

Bryan, W. B., A basalt-pantellerite association from Isla Socorro, Islas Revillagigedo, Mexico, in *Volcanoes and Tectonosphere*, edited by H. Aoki and S. Iizuka, pp. 75-91, Tokai Univ. Press, Tokyo, Japan, 1976.

Clague, D. A., Hawaiian alkaline volcanism, in *Alkaline Igneous Rocks*, edited by J. G. Fitton and B.G. J. Upton, *Spec. Publ. Geol. Soc. Am. 30*, 227-252, 1987.

Clark, S. C. L., and F. J. Spera, Evolution of the Miocene Tejeda magmatic system, Gran Canaria, Canary Islands, *Contrib. Mineral. Petrol.*, *104*, 681-699, 1990.

Crisp, J. A., Rates of magma emplacement and volcanic output, *J. Volcanol. Geotherm. Res.*, *20*, 177-221, 1984.

Crowe, B., and P. Crowe, *Heaven, Hell and Salt Water*, Adlard Coles, London, 1955.

Deino, A., and R. Potts, Single-crystal $^{40}Ar/^{39}Ar$ dating of the Olorgesailie Formation, southern Kenya Rift, *J. Geophys. Res.*, *95*, 8453-8470, 1990.

Druitt, T. H., and R. S. J. Sparks, A proximal ignimbrite breccia facies on Santorini, Greece, *J. Volcanol. Geotherm. Res.*, *13*, 147-171, 1982.

Duncan, R. A., and M. A. Richards, Hotspots, mantle plumes, flood basalts, and true polar wander, *Rev. Geophys.*, *29*, 31-50, 1991.

Eichelberger, J. C., Silicic volcanism: Ascent of viscous magmas from crustal reservoirs, *Annu. Rev. Earth Planet. Sci.*, *23*, 41-63, 1995.

Farmer, J. D., M. C. Farmer, and R. Berger, Radiocarbon ages of lacustrine deposits in volcanic sequences of the Lomas Coloradas area, Socorro Island, Mexico, *Radiocarbon*, *35*, 253-262, 1993.

Fisher, R. V., and H.-U. Schmincke, *Pyroclastic Rocks*, 472 pp., Springer-Verlag, New York, 1984.

Gerlach, D. C., Eruption rates and isotopic systematics of ocean islands: Further evidence for small-scale heterogeneity in the upper mantle, *Tectonophysics*, *172*, 273-289, 1990.

Graham, D. W., A. Zindler, M. D. Kurz, W. J. Jenkins, R. Batiza, and H. Staudigel, He, Pb, Sr and Nd isotope constraints on magma genesis and mantle heterogeneity beneath young Pacific seamounts, *Contrib. Mineral. Petrol.*, *99*, 446-463, 1988.

Henry, C. D., and J. A. Wolff, Distinguishing strongly rheomorphic tuffs from extensive silicic lavas, *Bull. Volcanol.*, *54*, 171-186, 1992.

Houghton, B. F., S. D. Weaver, C. J. N. Wilson, and M. A. Lanphere, Evolution of a Quaternary peralkaline volcano: Mayor Island, New Zealand, *J. Volcanol. Geotherm. Res.*, *51*, 217-236, 1992.

Howell, D. G., E. R. Schermer, D. L. Jones, Z. Ben-Avraham, and E. Scheibner, Preliminary tectonostratigraphic terrane map of the circum-Pacific region, *U.S. Geol. Surv. Open File Rep.*, 83-0716, 1985.

Lowenstern, J. B., and G. A. Mahood, New data on magmatic H_2O contents of pantellerites, with implications for petrogenesis and eruptive dynamics at Pantelleria, *Bull. Volcanol.*, *54*, 78-83, 1991.

Mahood, G. A., Pyroclastic rocks and calderas associated with strongly peralkaline magmatism, *J. Geophys. Res.*, *89*, 8540-8552, 1984.

Mahood, G. A., and W. Hildreth, Geology of the peralkaline volcano at Pantelleria, Strait of Sicily, *Bull. Volcanol.*, *48*, 143-172, 1986.

Mahood, G. A., and J. A. Stimac, Trace element partitioning in pantellerites and trachytes, *Geochim. Cosmochim. Acta*, *54*, 2257-2276, 1990.

Mammerickx, J., D. F. Naar and R. L. Tyce, The Mathematician paleoplate, *J. Geophys. Res.*, *93*, 3025-3040, 1988.

McClelland, L., E. Venzke, and J. Goldberg, Socorro (Mexico) Vesicular lava eruption from underwater vent W of the island, *Bull. Global Volcanism Network*, *18*, pp. 9-11, Smithson. Inst., Washington, D.C., 1993.

McDougall, I., and T. M. Harrison, *Geochronology and Thermochronology by the $^{40}Ar/^{39}Ar$ Method*, 212 pp., Oxford Univ. Press, New York, 1988.

Miller, D. S, I. R. Duddy, P. F. Green, A. J. Hurford, and C. W. Naeser, Results of interlaboratory comparison of fission-track age standards: Fission track workshop-1984, *Nucl. Tracks*, *10*, 383-391, 1985.

Norton, D., and H. P. Taylor, Quantitative simulation of the hydrothermal systems of crystallizing magma on the basis of transport theory and O isotope data: An analysis of the Skaergaard intrusion, *J. Petrol.*, *20*, 421-486, 1979.

Norton, D., H. P. Taylor, and D. K. Bird, The geometry and high-temperature brittle deformation of the Skaergaard Intrusion, *J. Geophys. Res.*, *89*, 10,178-10,192, 1984.

Richards, A. F., Geology of the Islas Revillagigedo, Mexico, 1, Birth and development of Volcan Barcena, Isla San Benedicto, *Bull. Volcanol., 22*, 75-123, 1959.

Schmincke, H.-U., Ash layers, hyaloclastites, and alteration of basaltic glass, *Deep Sea Drill Proj. Initial Rep., 65*, 477-486, 1983.

Self, S., The Recent volcanology of Terceira, Azores, *J. Geol. Soc. London, 132*, 645-666, 1976.

Shipboard Scientific Party, Guaymas Basin: Sites 477,478, and 481, *Deep Sea Drill Proj. Initial Rep., 64*, 211-416, 1982a.

Shipboard Scientific Party, Guaymas Basin: Sites 477,478, and 481, *Deep Sea Drill Proj. Initial Rep.*, 64, 417-504, 1982b.

Siebe, C., J. C. Komorowski, C. Navarro, J. McHone, H. Delgado, and A. Cortes, Submarine eruption near Socorro Island, Mexico: Geochemistry and scanning electron microscopy studies of floating scoria and reticulite. *J. Volcanol. Geotherm. Res., 68*, 239-271, 1995.

Smith, R. L., Ash-flow magmatism, *Spec. Pap. Geol. Soc. Am., 180*, 5-27, 1979.

Sparks, R. S. J., S. Self, and G. P. L. Walker, Products of ignimbrite eruptions, *Geology, 1*, 115-118, 1973.

Spell, T. L., and T. M. Harrison, The $^{40}Ar/^{39}Ar$ geochronology of post-Valles Caldera rhyolites, Jemez Volcanic Field, New Mexico, *J. Geophys. Res., 98*, 8031-8051, 1993.

Spera, F. J., and J. A. Crisp, Eruption volume, periodicity, and caldera area: Relationships and inferences on the development of compositional zonation in silicic magma chambers, *J. Volcanol. Geotherm. Res., 11*, 169-187, 1981.

Steiger, R. H., and E. Jager, Subcommission on geochronology: Convention on the use of decay constants in geochemistry and cosmochemistry, *Earth Planet. Sci. Lett., 36*, 359-362, 1977.

Taylor, J. R., *An Introduction to Error Analysis*, 270 pp., Univ. Sci., Mill Valley, Calif., 1982.

Walker, G. P. L., Origin of coarse lithic breccias near ignimbrite source vents, *J. Volcanol. Geotherm. Res., 25*, 151-171, 1985.

Wendt, I., and C. Carl, The statistical distribution of the mean squared weighted deviation, *Chem. Geol.*, 86, 275-285, 1991.

York, D., Least squares fitting of a straight line with correlated errors, *Earth Planet. Sci. Lett., 5*, 320-324, 1969.

W. A. Bohrson, Department of Geological Sciences, University of California, Santa Barbara, CA 93106. (e-mail: bohrson@magic.geol.ucsb.edu)

A. L. Grunder, Department of Geosciences, Oregon State University, Corvallis, OR 97331. (email: grundera@bcc.orst.edu)

T. M. Harrison and M. R. Reid, Department of Earth and Space Sciences, University of California, Los Angeles, CA 90095. (e-mail: tmh@argon.ess.ucla.edu; reid@zephyr.ess.ucla.edu)

M. T. Heizler, New Mexico Bureau of Mines and Mineral Resources, Socorro, NM 87801. (email: matt@mailhost.nmt.edu)

J. Lee, Geology Department, Central Washington University, Ellensburg, WA 98926. (email: leej@picante.geology.cwu.edu)

(Received December 15, 1994; revised January 16, 1996;
accepted January 23, 1996)